

Final Report to

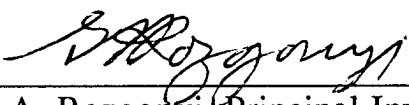
Electronic Systems Division
Hanscom AFB, MA 01731-5000

For Research Entitled:

**Non-Destructive X-Ray, Optical and Electrical
Materials Characterization Techniques
for Silicon-on-Insulator (SOI) Technology**

Covering the Period From April 1, 1990 to Sept. 30, 1993

Submitted by:



G.A. Rozgonyi, Principal Investigator

North Carolina State University
Materials Science and Engineering Dept.
Raleigh NC 27695-7916

Ph. (919) 515-2934, FAX (919) 515-5115, e-mail Rozgonyi@mte.ncsu.edu

DTIC QUALITY INSPECTED 8

19950623 009

Final Report to

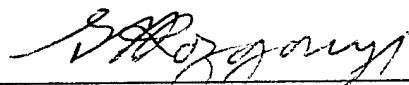
Electronic Systems Division
Hanscom AFB, MA 01731-5000

For Research Entitled:

**Non-Destructive X-Ray, Optical and Electrical
Materials Characterization Techniques
for Silicon-on-Insulator (SOI) Technology**

Covering the Period From April 1, 1990 to Sept. 30, 1993

Submitted by:


G.A. Rozgonyi, Principal Investigator

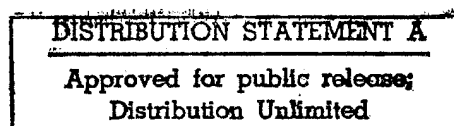


North Carolina State University
Materials Science and Engineering Dept.
Raleigh NC 27695-7916

Ph. (919) 515-2934, FAX (919) 515-5115, e-mail Rozgonyi@mte.ncsu.edu

19950623 009

DTIC QUALITY INSPECTED 8



NON-DESTRUCTIVE SOI PROCESS EVALUATION USING RECOMBINATION LIFETIME MEASUREMENTS

A. Buczkowski, F. Shimura, and G. A. Rozgonyi
Department of Materials Science and Engineering
North Carolina State University
Raleigh, NC 27695-7916

and

B. Cordts
IBIS Technology Corporation
32A Cherry Hill Drive
Danvers, MA 01923

The properties of the buried Si-SiO₂ interface, the concentration of structural defects, and the level of contamination have been monitored nondestructively via their effect on the surface and bulk components of recombination lifetime by a laser/ microwave photoconductance technique. It has been found for single and multiple implant/ anneal SIMOX material that the bulk recombination lifetime decreases if the annealing alone (no implantation), or both implantation and annealing processes are applied. However, a bulk lifetime recovery for multiple implant/ anneal process is observed after the second and third processing steps. In addition, the superficial layer and Si-SiO₂ interface still contain a very high density of electrical defects even after the structural damage removing/ oxide forming high temperature treatment. This defect density results in a surface recombination velocity on the order of 1000 cm/s, two or three orders of magnitude more than a surface subjected to annealing alone (without implantation), and only one order less than non-annealed, implanted material.

INTRODUCTION

The non-destructive full wafer evaluation of SOI/SIMOX is a very desirable factor in the further development of this new material for semiconductor device technology. It is particularly important to track the properties of the superficial layer, buried Si-SiO₂ interface, the concentration of structural defects, and the level of contamination introduced during the extended exposure ion-implantation and/ or prolonged high temperature annealing heat treatment. Because minority carrier lifetime measurements are sensitive to both chemical and structural defects, including point-defect complexes and contaminants, the contactless laser excitation/ microwave reflection photoconductance (LM-PC) method^{1,2} has been extensively used at North Carolina State University^{3,4,5} for evaluation of bulk and surface material properties. The LM-PC is used to independently separate the recombination properties of a SIMOX substrate and its buried oxide-substrate interface.⁶ The recombination properties of the top superficial silicon layer are estimated by comparison of two decays derived by measuring a sample excited first from the front and then from the back side, as shown in Fig. 1. The contribution from the top superficial layer in the front illumination experiment depends on the layer quality and the ratio of photon energy absorbed within the layer to the energy absorbed within the substrate. This ratio strongly depends on the laser wavelength used and the Si/SiO₂ layer thicknesses because of

Accession For	
NTIS	CRA&I <input checked="" type="checkbox"/>
DTIC	TAB <input type="checkbox"/>
Unannounced <input type="checkbox"/>	
Justification _____	
By _____	
Distribution / _____	
Availability Codes	
Dist	Avail and/or Special
A-1	

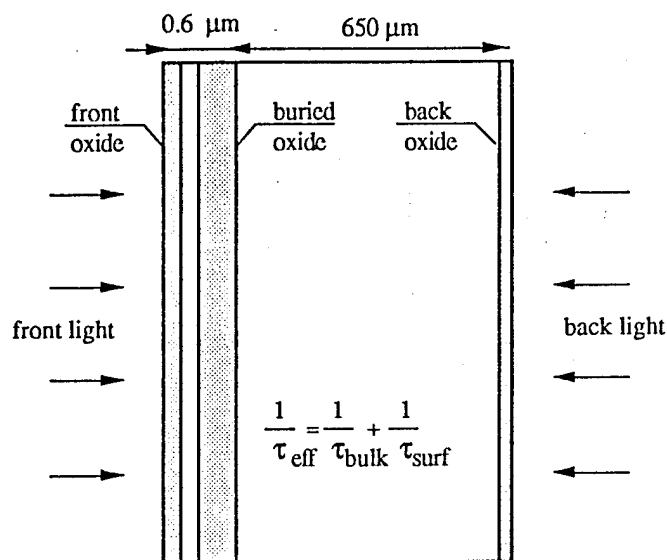


Fig. 1. Schematic cross section of SIMOX wafer measurement configurations

multiple reflection at the Si/SiO₂ and SiO₂/Si interfaces. If favorable conditions are met, it is the recombination properties of the superficial layer, the Si-SiO₂ interfaces of the buried oxide, the Si-SiO₂ interfaces of the front and back side oxide grown before ion implantation and during post implantation annealing, and finally the bulk recombination which are responsible for signal decay. In the experiment with back side excitation, the decay is much less affected by the front superficial silicon layer since the energy which is absorbed there is very low. In this case, the quality of buried oxide-substrate and back side oxide-substrate interfaces, along with the bulk recombination, but not the superficial layer itself, affect the signal decay.

Taking into account the above experimental conditions, we interpret minority carrier recombination due to the Si-SiO₂ interface and superficial layer as a "surface" effect, and that due to the bulk defects as "bulk" recombination. These two recombination processes make up the effective lifetime τ_{eff} ; however, after appropriate analysis^{6,7}, the separate lifetime components can be determined. The difference in surface lifetime component when measured at front and back illumination is a measure of the superficial layer quality. Although the recombination properties of the top superficial layer are not yet directly calculated in this initial LM-PC experiment, we believe that the bulk recombination lifetime within the substrate and surface recombination velocity reflect the dynamics of the properties following processing of SIMOX material and can be used for monitoring the quality of implantation and annealing equipment.

EXPERIMENT

The SIMOX substrates were produced by IBIS Technology Corp. by oxygen implantation into silicon material preheated to 450 °C. In the initial wafer sequence examined, four n-type, 5-inch diameter, and eight p-type, 4-inch diameter, 10 Ωcm CZ silicon wafers were processed, as illustrated in Fig. 2 and 3. The implant energy was 200 keV and the multiple dose sequence was $(0.55 + 0.55 + 0.9) \times 10^{18} \text{ cm}^{-2}$.

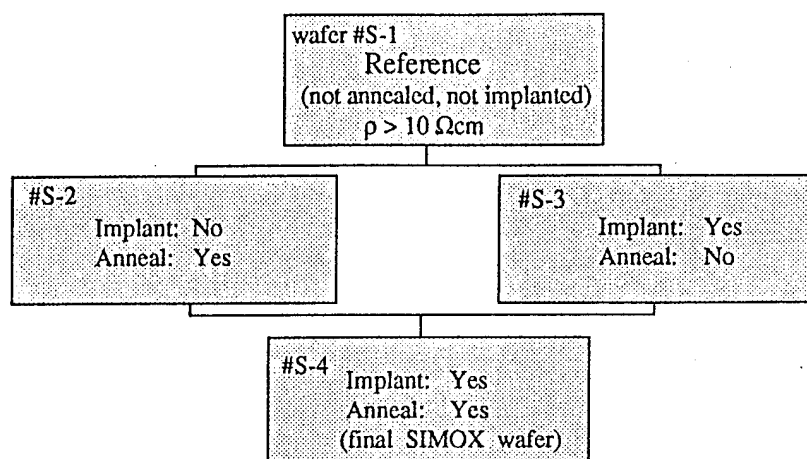


Fig. 2. Schematic diagram showing the preparation sequence and sample identification for evaluation of the single implant/ anneal SIMOX samples

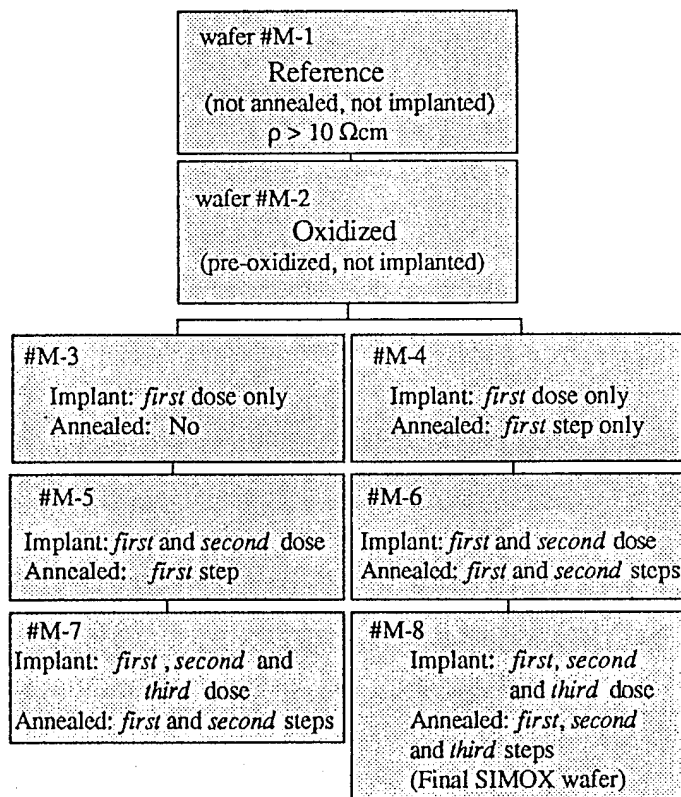


Fig. 3. Schematic diagram showing the preparation sequence for evaluation of the multiple implant/ anneal SIMOX samples

Each implantation step was followed by a 1310 °C, 5-hour annealing in an Ar + 0.5% O₂ ambient. For single implant/ anneal SIMOX (S-SIMOX) a full oxygen dose and one step annealing were applied. The multiple implant/ anneal SIMOX (M-SIMOX) wafers were initially oxidized to grow a 20 nm thick oxide to reduce the surface recombination to a negligible level, i.e. on the order of 0.1 cm/s to 1 cm/s. The influence of SOI processing on the LM-PC signal decay was tracked for each processing step illustrated in Figs. 2 and 3 and the lifetime values were semi-quantitatively evaluated.

RESULTS

In the following discussion we used the letters S and M for single and multiple implant/ anneal samples, respectively; and F and B for the front and back side illumination conditions. Thus, the description SF-4 denotes results obtained for the single implant/ anneal wafer S-4, see Fig. 2, measured with the laser light pulsed at the front side. Initially, the uniformity of the fully processed sample M-8 was evaluated via a full wafer mapping of thickness and effective lifetime, as shown in Figs. 4a and b, respectively. Thus the MF-8 lifetime and the superficial layer thickness contours were compared. It was found that the lifetime increases with the superficial layer thickness. This correlation was observed whether front or back side illumination was used. The observed effect is actually not simply related to the layer thickness (which may control the surface component of recombination lifetime while measured at front illumination), but also to a different dose of impurity introduced during implantation and redistributed during annealing. A qualitatively similar correlation was observed for sample S-4 by comparing the lifetime map with the distribution of interference fringes observed using visual wafer inspection.

Following the initial uniformity measurements, the influence of ion implantation and furnace annealing on the minority carrier decay for the S samples was recorded, as presented in Fig.5. The degrading influence of furnace annealing on the minority carrier decay is evident for SF-2 for which the effective lifetime decreased by a factor of 5 from $\tau_{\text{eff}} \approx 35 \mu\text{s}$ to $\tau_{\text{eff}} \approx 7 \mu\text{s}$, while the bulk lifetime, obtained after lifetime component separation⁶, decreased by two orders of magnitude from 1 ms to 8 μs , as measured at room temperature. Since the bulk lifetime is directly related to the trap concentration and/or location within the bandgap, it is evident that a significant increase in defect or impurity related traps occur during the post-implantation annealing. Annealing a non-implanted reference wafer, e.g. sample SF-2, degrades τ_{bulk} from about 1 ms to 32 μs , compare samples SF-2 and SF-3. Samples which were both implanted and annealed undergo a further bulk lifetime decrease to 8 μs , see sample SF-4 in Fig. 5. Moreover, both implanted samples, whether they are annealed or not, have a Si-SiO₂ interface characterized with relatively low surface lifetime, $\tau_{\text{surf}} \approx 36 \mu\text{s}$ and $\tau_{\text{surf}} \approx 42 \mu\text{s}$, which corresponds to a surface recombination velocity $S > 10^4 \text{ cm/s}$ or $S \approx 3 \cdot 10^3 \text{ cm/s}$ for SF-3 and SF-4, respectively. Thus, the annealing process does not fully remove the defects/ impurities within the superficial layer and/or at the buried oxide-silicon substrate interface. Recall that for MOS quality oxide-silicon interfaces S typically ranges from 0.1 cm/s to 10 cm/s⁸, and a value below the detection limit (100 cm/s) is observed on the non-implanted and annealed sample SF-2. The same samples were also measured with back side laser illumination and decays similar to their front illumination counterparts were obtained for samples SB-2 and SB-3, while the sample SB-4 was much different from the SF-4 and characterized with much lower (below detection limit) surface recombination velocity. Therefore, it can be concluded that the "surface" effect observed in sample SF-4 may come from enhanced recombination rate within the superficial layer but does not have to be related to the poor

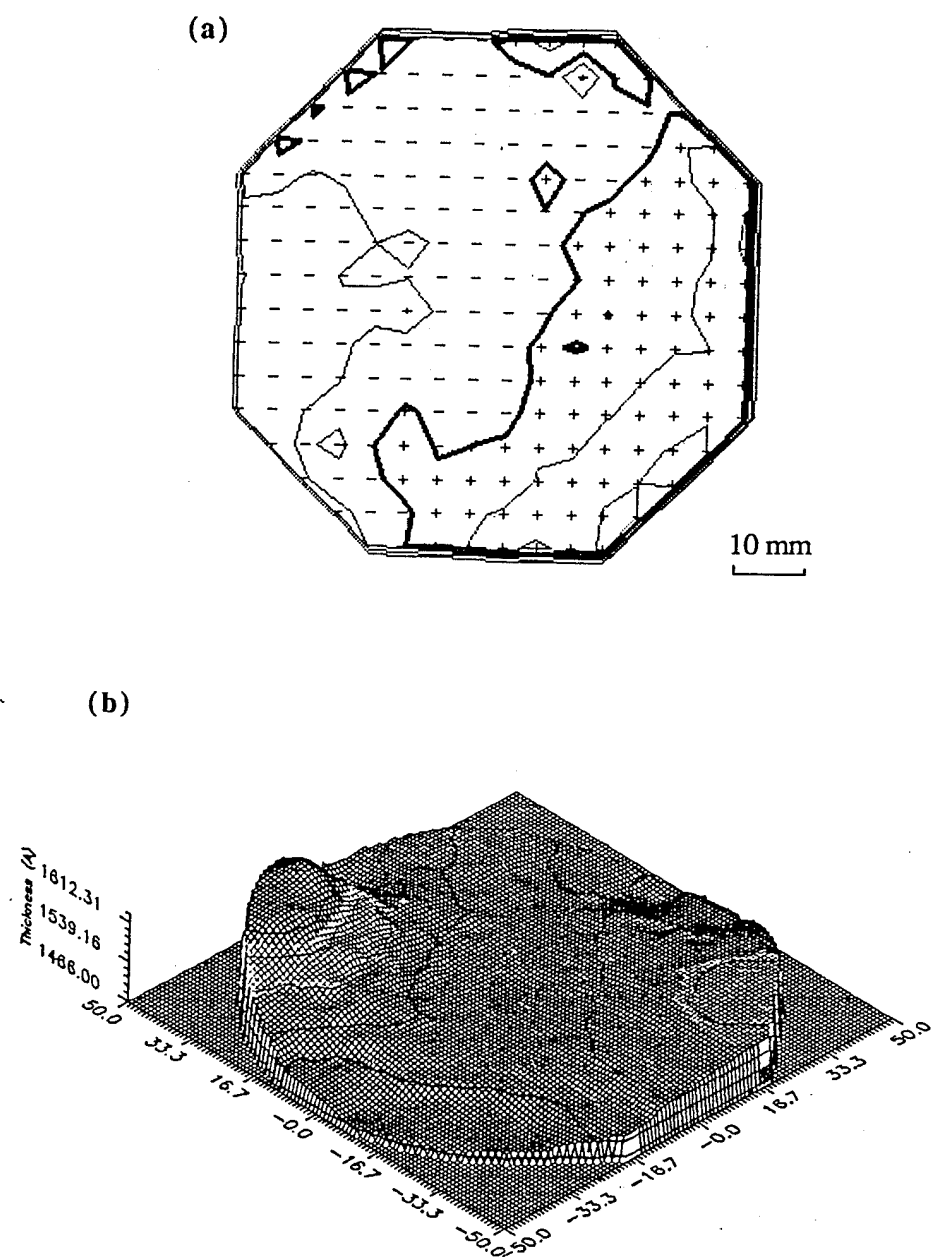


Fig. 4. (a) Recombination lifetime and (b) thickness distribution of the final multiple implant/ anneal SIMOX material. Notice that (b) is rotated counterclockwise 45° with respect to (a).

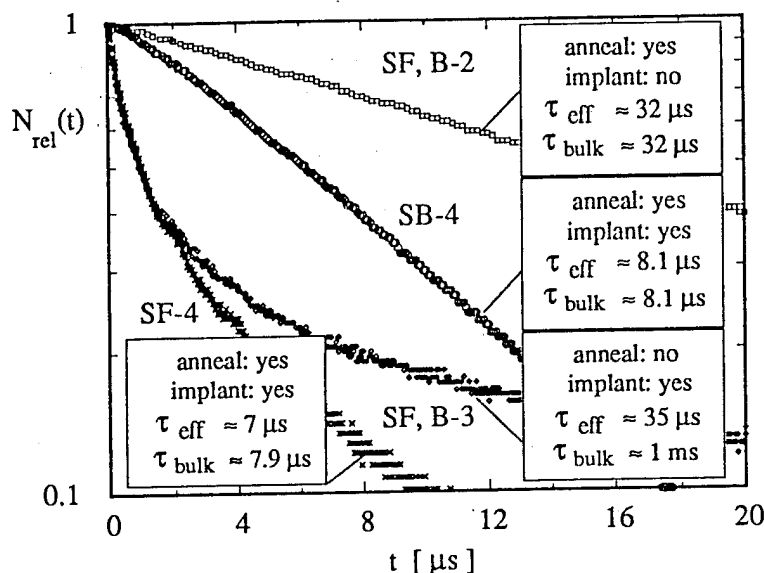


Fig. 5. Normalized minority carrier decays of S-SIMOX wafers measured on post-implantation annealed and non-annealed samples

electrical properties of the Si-SiO₂ interfaces of the buried oxide itself. Notice that due to very low thickness of the superficial layer, the surface component of the effective lifetime can be lower than the bulk value, even at relatively low surface recombination velocity, since τ_{surf} is proportional to the layer thickness d ($\tau_{surf} = d / 2 S$).

It was expected that an improvement in the superficial layer and buried silicon-oxide interface would be obtained when a multiple implant/ anneal processing sequence was used. However, the results indicate that a simple cumulative sum of individual implantation/ annealing steps can not be used. A typical family of carrier decays characteristic for initial M-SIMOX material and after the first implantation/ annealing step is presented in Fig. 6. The decays are very similar to those observed for S-SIMOX, although the absolute values are different, due to different starting material and processing conditions. The main conclusion from Fig. 6 is that lifetime degrades after both ion implantation and annealing, compare MF-2, MF-3 and MF-4, and that the top superficial layer after the first implantation/ annealing cycle is characterized with high recombination rate, compare MF-4 and MB-4. However, second and third implantation/ annealing do not deteriorate but significantly improve the effective recombination lifetime, as shown in Fig. 7. Therefore, metal impurities introduced during implantation/ annealing are not solely responsible for lifetime, since in such a case continued deterioration should be observed. The bulk lifetime is affected both by implantation damage and SiO₂ phase formation after annealing. After the first dose implantation/ annealing a layer of SiO₂ precipitations is observed, surrounded by material characterized by high mechanical tension and structural disorder⁹ which results in a low lifetime value. Each consecutive implantation/ annealing improves buried oxide quality, which finally isolate substrate from the top superficial layer and decreases the total recombination rate. The quality of the superficial layer itself also improves, as the amount of defective silicon trapped within buried oxide decreases, and a

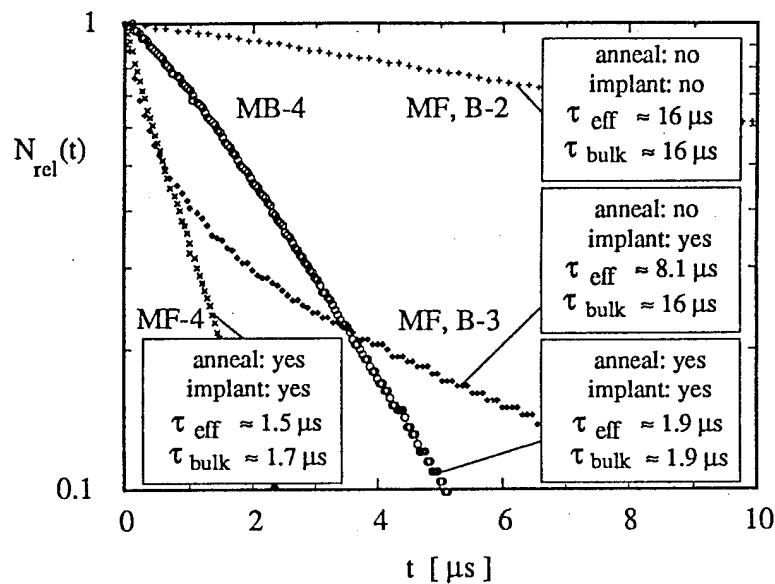


Fig. 6. Normalized minority carrier decays of M-SIMOX wafers measured on the first step post-implantation annealed and non-annealed samples

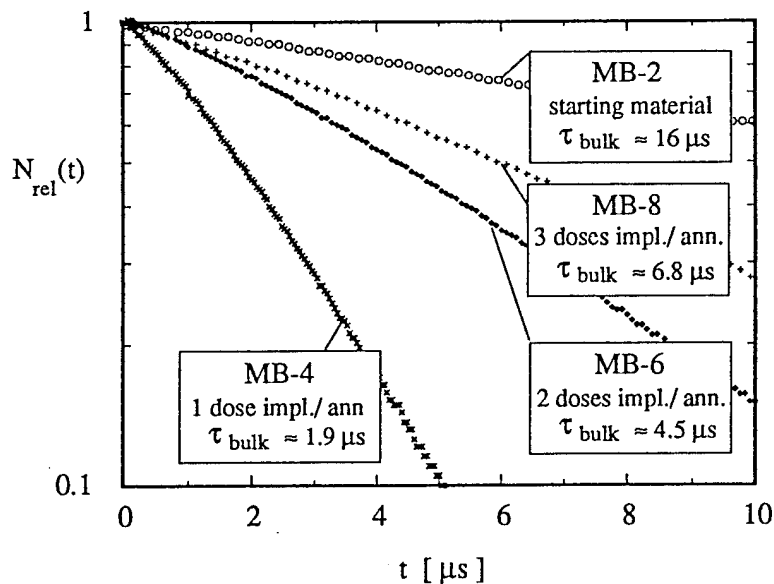


Fig. 7. Normalized minority carrier decays of M-SIMOX wafers showing τ_{bulk} value measured after each implantation/annealing step

continuous and sharp SiO_2 layer is formed. At the same time impurities from the substrate and superficial layer are possibly getered at the silicon-oxide interfaces. As a result the final quality of the superficial layer achieved in the multiple process, presumed as a "surface"

recombination velocity measured at front illumination, is of the order of $1-2 \cdot 10^3$ cm/s. This is about two times lower than that observed in a single implantation/ annealing process. It seems that it is still too high when compared to the non-implanted samples SB-2 or MB-2, which were below the detection limit of the LM-PC technique (100 cm/s).

The temperature dependence of the recombination properties of traps introduced during implantation/ annealing processes provides an additional insight into the quality of SIMOX material. According to the Shockley-Read-Hall theory (SRH), the probability of recombination is the highest for traps occupying deep levels, i.e., close to the middle of band gap; and decreases significantly for shallower energy levels. Thus, trap energy levels are a characteristic property of a given defect structure and in certain cases can be used to isolate the chemical or structural source of the trap. It is possible to determine energy levels via the recently developed LM-deep level transient spectroscopy (LM-DLTS)¹⁰ technique, wherein the surface and bulk lifetime are measured over a wide range of temperature permitting the energy levels of deep states to be calculated. For this calculation, the energy level influence on the observed lifetime can be evaluated, as predicted by the SRH theory.

A comparison of the dependence of the bulk component of lifetime versus inverse temperature for non-annealed and annealed S-SIMOX wafers is presented in Fig. 8.

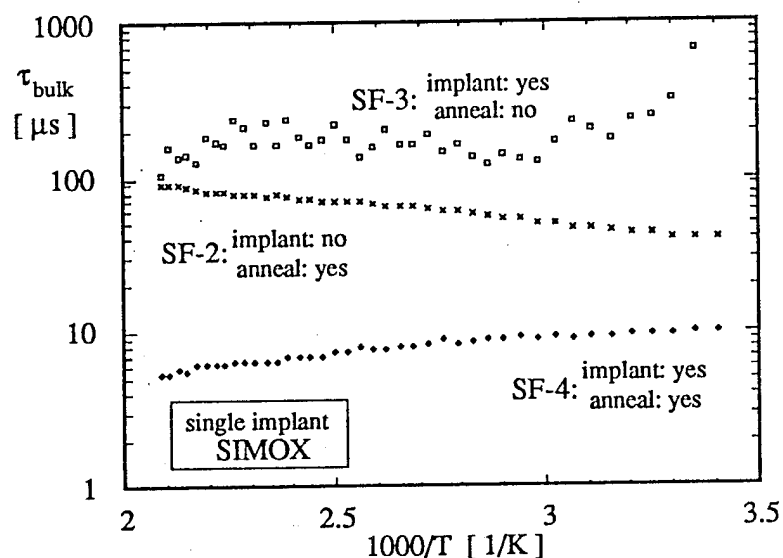


Fig. 8. Temperature dependence of the bulk lifetime measured on post-implantation annealed and non-annealed samples

Note that, as expected, the bulk lifetime value is strongly affected by the annealing process. Essentially no influence of measurement temperature on the bulk lifetime is observed on samples SF-3 and SF-4 subjected to implantation. This behavior is typical for materials with a high density of structural defects. For the non-implanted, but annealed sample SF-2 an increase of lifetime with temperature is observed which is typical for samples contaminated with metals.¹¹ The temperature dependence of surface recombination velocity for sample SF-3 (not annealed), see Fig.9, indicates that S is almost constant and very high, of the order of 10^4 cm/s, characteristic of a surface heavily damaged after

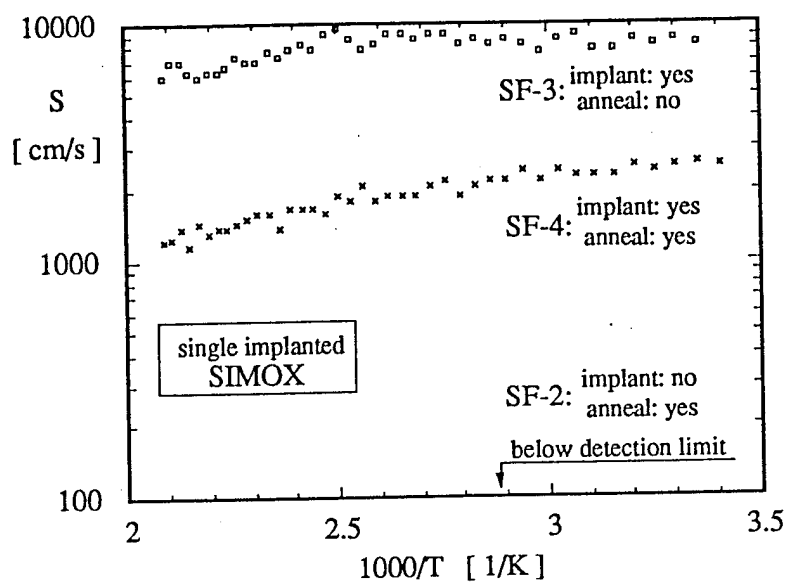


Fig. 9. Temperature dependence of surface recombination velocity measured on post-implantation annealed and non-annealed samples

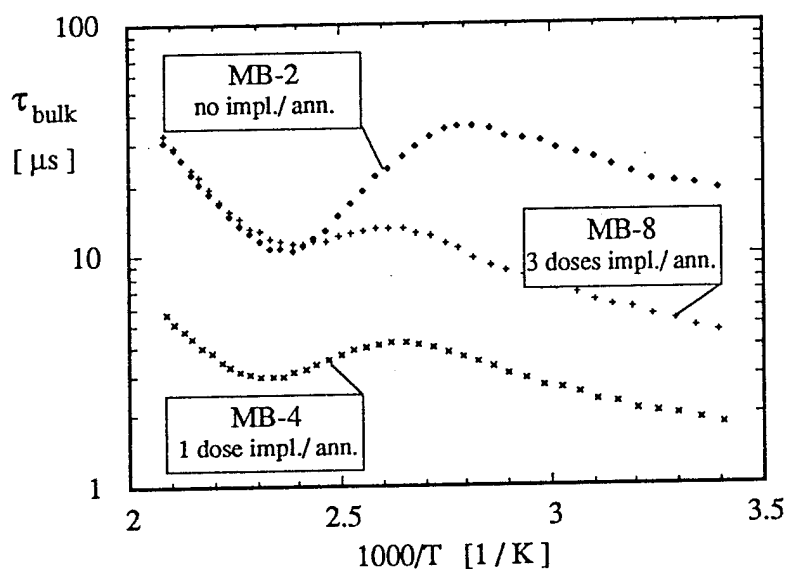


Fig. 10. Temperature dependence of the bulk lifetime measured on M-SIMOX samples annealed after different implantation steps

ion-implantation; whereas for sample SF-4 the lower surface recombination velocity and larger dependence on temperature is typical of surfaces containing shallower defects. The temperature dependence of the bulk lifetime component of reference M-SIMOX material, and that measured after first and third implantation/ annealing cycles is shown in Fig. 10.

In spite of the lifetime level changes, the observed curves are characterized with a specific shape, showing a broad peak and a depression, which can be attributed to the dissociation of iron-boron (Fe_iB_s) pairs, as studied in Ref. 12. All measured samples were contaminated with iron including the starting material, and the iron concentration increased one order of magnitude after the first implantation/ annealing step. The initial iron concentration of 10^{12} cm^{-3} can be estimated by comparing the results observed here to those presented in Ref. 12. Since lifetime increases after the second and third annealing, especially for the high temperature range where deeper states controls lifetime, e.g. iron in interstitial position, it seems that gettering mechanisms must once again be taken into account.

SUMMARY

The properties of the buried Si-SiO₂ interface and the bulk substrate have been monitored nondestructively via their effect on the surface and bulk components of recombination lifetime using a laser/ microwave photoconductance (LM-PC) technique. It has been found for single implant/ anneal SIMOX material that the bulk recombination lifetime decreased from 1 ms, characteristic of an initial silicon substrate, to 35 μs or to 8 μs if the annealing alone (no implantation), or both implantation and annealing processes have been applied, respectively. A similar degradation is observed for multiple implanted/ annealed material, but only after the first implantation/ annealing. A lifetime recovery is observed after the second and third step. Moreover, the superficial silicon and the Si-SiO₂ interface still contain a very high density of electrical defects even after a surface oxide forms during the high temperature treatment. This defect density results in a surface recombination velocity on the order of 1000 cm/s, two or three orders of magnitude more than a surface subjected to annealing alone (without implantation), and only one order less than a non-annealed implanted sample. Since in the multiple implant/ anneal SIMOX process the superficial layer quality improvement is observed after the second and third implantation/ annealing cycles it seems that further progress can be achieved by upgrade of annealing conditions.

REFERENCES

- ¹ D.K. Schroder, *Semiconductor Material And Device Characterization*, 359-448, (John Wiley & Sons, New York, 1990).
- ² J. W. Orton and P. Blood, *The Electrical Characterization of Semiconductor: Measurement of Minority Carrier Properties*, (Academic Press, San Diego, 1990).
- ³ F. Shimura, T. Okui, and T. Kusama, *J. Appl. Phys.* **67**, 7168 (1990).
- ⁴ Y. Kirino and F. Shimura, *J. Appl. Phys.* **69**, 2700 (1991).
- ⁵ A. Buczkowski, Y. Kirino, T. Zhou, Z. Radzimski, D. Finn, L. Hellwig, J. Rossi, G. Rozgonyi and F. Shimura, in *Defects in Silicon II* (Eds. W. M. Bullis, W. Gosele, and F. Shimura, The Electroch. Soc., 1991), pg.107
- ⁶ A. Buczkowski, Z. Radzimski, G. Rozgonyi and F. Shimura, *J. Appl. Phys.*, **69**, 6495 (1991).
- ⁷ K. L. Luke and L. J. Cheng, *J. Appl. Phys.* **61**, 2282 (1987).
- ⁸ A. S. Grove, *Physics and Technology of Semiconductor Devices*, pg.144, pg. 334 (John Wiley & Sons, New York, 1967).
- ⁹ A. Belogorokhov, A. Danilin, Y. Erokhin, A. Kalinin, V. Mordkovich, V. Saraikin and I. Khodos, *Nucl. Instr. and Methods in Phys. Res.* **B55**, 750 (1991)
- ¹⁰ Y. Kirino, A. Buczkowski, Z. Radzimski, G. Rozgonyi and F. Shimura, *Appl. Phys. Lett.*, **57**, 2832 (1990)
- ¹¹ A. Buczkowski, Z. Radzimski, Y. Kirino, F. Shimura, and G. Rozgonyi, *MRS Symp. Proc.*, **209**, 567 (Mat. Res. Soc., Pittsburgh, 1991)
- ¹² Y. Hayamizu, T. Hamaguchi, S. Ushio, T. Abe, and F. Shimura, *J. Appl. Phys.*, **69**, 3077 (1991).

CORRELATION BETWEEN X-RAY MOIRE' PATTERN AND DISLOCATION DENSITY IN SIMOX WAFERS

M. K. El-Ghor and K. A. Joyner
Texas Instruments, Inc.; Dallas, Texas 75265

and

G. A. Rozgonyi
Department of Materials Science and Engineering,
North Carolina State University;
Raleigh, North Carolina 27695-7916

Abstract

Singly and multiply implanted SIMOX wafers were evaluated using Lang transmission x-ray topography as well as chemical etching. Moire' patterns were clearly observed in the multiply implanted material and some areas in the singly implanted ones. The presence of Moire' patterns indicates high quality SIMOX material. Direct correlation was made between different areas of the x-ray topographs and dislocation density using the SECCO solution. It is found that wafers exhibiting no Moire' patterns have dislocation densities greater than $8 \times 10^6/\text{cm}^2$, while others with strong Moire' fringes have dislocations two orders of magnitude less. Although the difference in the density of defects is not substantial, a clear trend is established between the presence of Moire' fringes and dislocation density. This demonstrates the capability of x-ray topography to screen SIMOX material before further processing.

Introduction

Silicon-on-insulator structures produced by Separation by IMplantation of OXygen (SIMOX) provides a powerful technique to build high speed, radiation hardened integrated circuits [1]. A large number of studies have been carried out over the years to evaluate SIMOX material using transmission electron microscopy (TEM), secondary ion mass spectroscopy (SIMS), and Auger electron spectroscopy (AES) [2]. Recently, x-ray topography (XRT) was employed to evaluate the crystallographic perfection of the substrate silicon and the superficial layer in SIMOX [3,4]. Due to the inherently nondestructive nature of XRT, annealed SIMOX wafers can be screened using this technique before further processing. In this report, a correlation is presented for the first time between XRT and dislocation density.

Experimental

Single and multiple implant SIMOX structures were produced by implanting 4" N-type Si(100) wafers at 200 keV with doses of $1.8 \times 10^{18}/\text{cm}^2$ and $(0.75 + 0.75) \times 10^{18}/\text{cm}^2$, respectively. The ion implanter used was an Eaton NV-200, operating with a beam current of 40 mA and an implant temperature of 620 C. The wafers were capped with 300 nm of plasma oxide, which was densified before annealing. SIMOX annealing was done at 1325 C for 5 hours in an Ar+1%O₂ ambient. Following the anneal a 4 μm of silicon epitaxial layer was grown on the SIMOX substrates to enhance the intensity of fringe contrast (if any) obtained from the XRT patterns. Two singly and two multiply implanted wafers were selected for characterization. The lattice displacement of the epi-/SIMOX wafers were imaged via transmission x-ray topography (XRT) under different diffraction conditions using Mo K α radiation. Then, specific areas were carefully selected from these wafers and etched with the Secco solution [5] to delineate the extended defects and finally correlate the defect distribution with the XRT results. It should be noted that nine samples were etched from each of three half wafers to determine the dislocation densities. However, 12 samples were taken from wafer D, as indicated in figure 1(d).

Results and Discussion

Figure 1 shows x-ray transmission topographs of all four wafers taken with g_{220} . Very distinct Moire' fringes are observed in figure 1(b and c), for the multiply implanted wafers, formed by the silicon substrate and superficial Si with its epitaxial layer. This is indicative of low defect density material since the presence of highly defective areas, which contain many dislocations, will suppress the formation of the Moire' fringe contrast due to the large local lattice displacement and resultant intensity increase induced by the dislocations (4).

The correlation between the presence of the Moire' pattern and dislocation density is established by the etching results. The average dislocation density in these two wafers is $7.0 \times 10^4/\text{cm}^2$ and $2.0 \times 10^4/\text{cm}^2$, respectively, as shown in table 1. These two wafers showed strong Moire' patterns. However,

Sample	Wafer #	Dose x $E18$	Discl. Density	Moire' Pattern
A	F 152	1.8	4E7	None
B	F 635	.75+.75	7E4	Yes
C	F 601	.75+.75	2E4	Yes
D	F 910	1.7	3-8E6	Patchy

Table 1 Moire' pattern intensity and dislocation densities

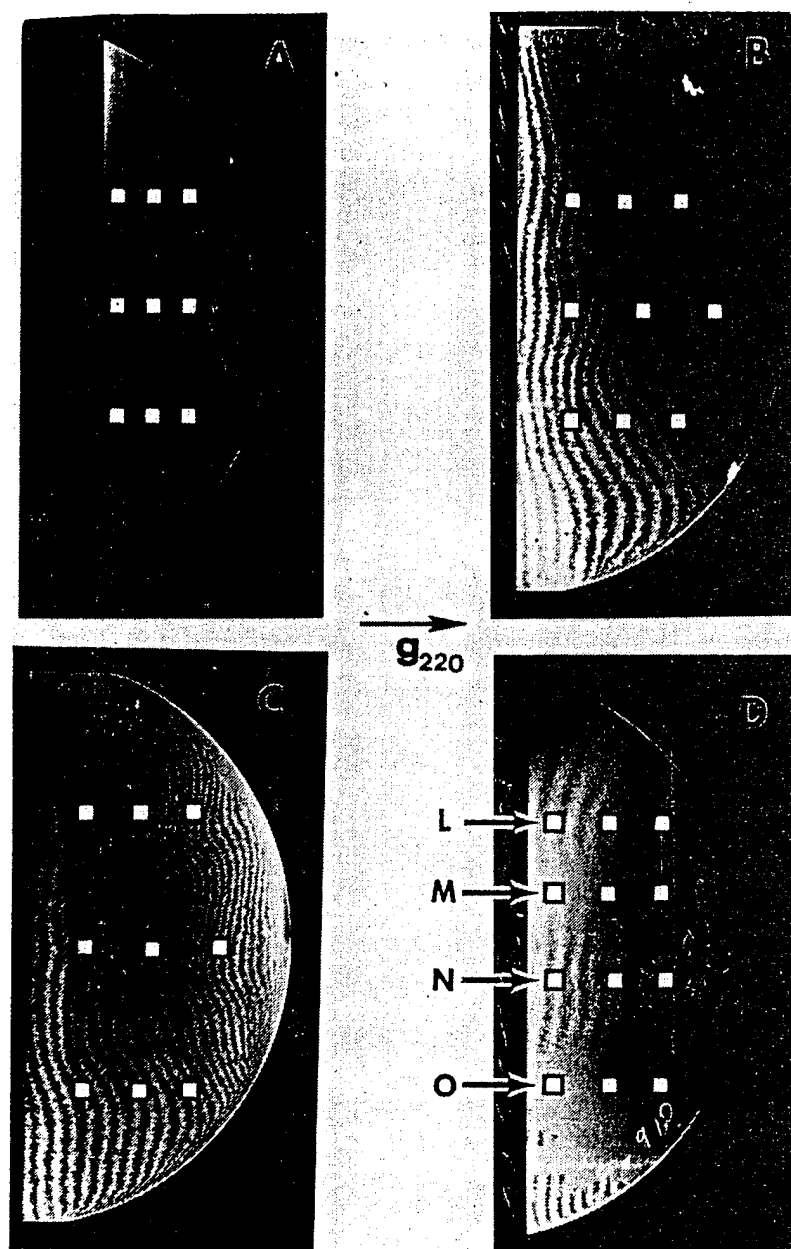


Figure 1. X-ray transmission topographs taken with Mo K α 1-g220:
 (a) $1.8 \times 10^{18}/\text{cm}^2$, (b) and (c) $(0.75 \pm 0.75) \times 10^{18}/\text{cm}^2$. The squares
 mark the area subsequently etched with Secco solution. In wafer (d),
 regions L and N exhibit Moiré' pattern, M shows weak but visible pattern,
 while O shows no fringes.

no Moire' fringes were observed in figure 1(a) which corresponds to the wafer implanted with a dose of $1.8 \times 10^{18}/\text{cm}^2$. As expected, the etch pit results revealed a high dislocation density of $4.1 \times 10^7/\text{cm}^2$. Figure 2 shows SEM micrographs of dislocation etch pits after the Secco etch of wafers A and C.

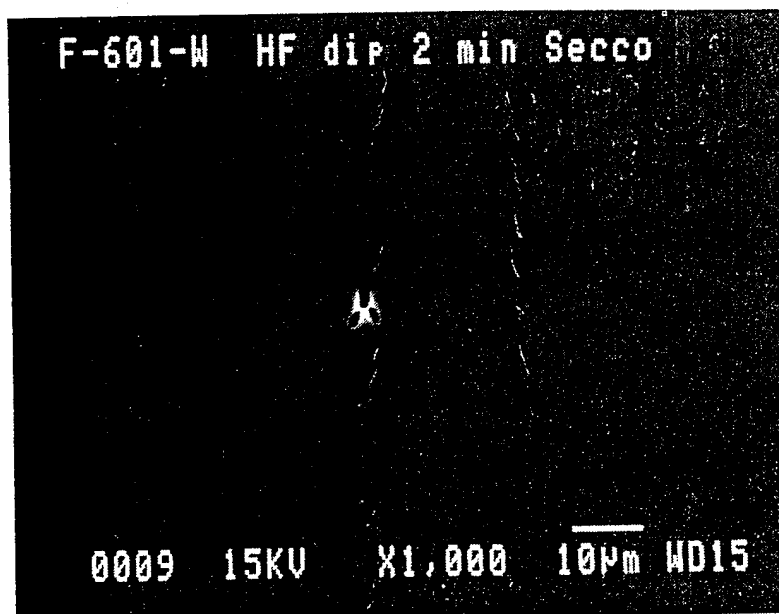
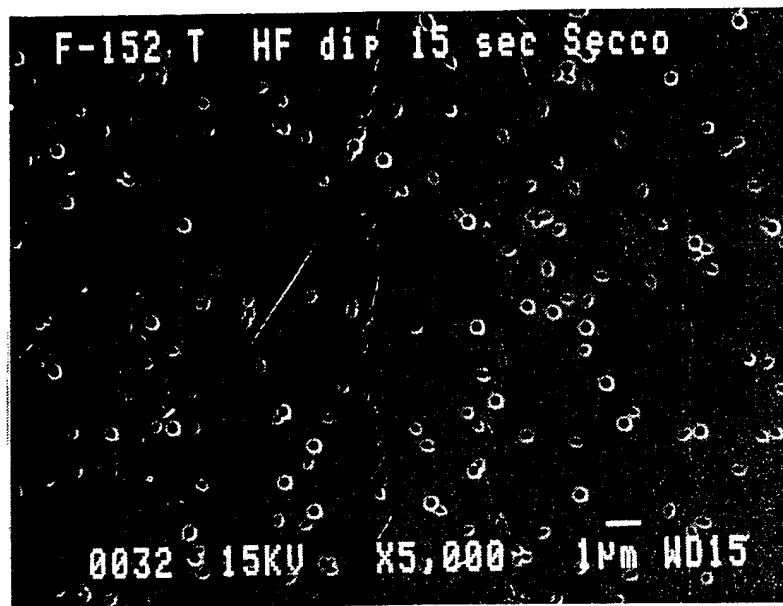


Figure 2. SEM micrographs of: (a) Wafer A showing dislocation etch pit density of $4 \times 10^7/\text{cm}^2$, and (b) Wafer C with an etch pit density of $2 \times 10^4/\text{cm}^2$.

The x-ray topograph of the other wafer implanted with a single dose is shown in fig. 1(d). The fact that this wafer provided different patterns: Moire' fringes, weaker ones, and no fringes served as an ideal sample for developing a one-to-one correspondence between XRT and etch pit dislocation density. Three samples were obtained from each of the four areas labelled L, M, N, and O in fig. 1(d) (the fourth area is the additional region (L) exhibiting a Moire' pattern). Then all samples were etched for 30 seconds in Secco solution. The dislocation densities corresponding to L, M, N, O, are 4.5 , 6.3 , 3.3 , and $7.8 \times 10^6/\text{cm}^2$, respectively. It is apparent that there is a trend in the density of defects with respect to the presence of Moire' fringes. The two areas, L and N, which exhibit the Moire' fringes show the lowest defect density. This is followed by the weak fringe area M with a higher density of $6.3 \times 10^6/\text{cm}^2$, followed by area O with no fringes, having the highest defect density of the four.

It should be noted that the Moire' fringes observed in wafer (d) are weaker than these in either (b) or (c). This is supported by the etching data where the dislocation density in (d) is about two orders of magnitude higher than the other two wafers. Thus, the intensity of the Moire' fringes is indicative of the quality of the material. Finally, the correlation between the dislocation density and the Moire' fringes obtained from all four wafers under study sets an upper limit of dislocation density which is consistent with production of a Moire' pattern.

ACKNOWLEDGEMENTS

This work was supported by the WL/MTEM under Contract No. F33615-89-C-5714.

REFERENCES

1. H. W. Lam, R. F. Pinizzotto, and A. F. Tasch, Jr., in VLSI Handbook edited by N. G. Einspruch (Academic, Orlando, FL, 1985), p.503.
2. C. G. Tuppen, M. R. Taylor, P. L. F. Hemment, and R. P. Arrowsmith, Appl. Phys. Lett., 45, 57 (1984).
3. G. A. Rozgonyi, Z. J. Radzimski, T. Higuchi, B. L. Jiang, D. M. Lee, T. Zhou, D. Schmidt, and J. Blake, Appl. Phys. Lett. 55, 586 (1989).
4. B. L. Jiang, F. Shimura, and G. A. Rozgonyi, Appl. Phys. Lett. 56, 352 (1990).
5. F. Secco D'Aragona, J. Electrochem. Soc. 119, 948 (1972).

Dependence of Minority-Carrier Recombination Lifetime on Surface Microroughness in Silicon Wafers

Hiroshi DAIO* and Fumio SHIMURA

Department of Materials Science and Engineering, North Carolina State University, Raleigh, NC 27695-7916, USA

(Received September 9, 1993; revised manuscript received October 28, 1993; accepted for publication November 20, 1993)

The influence of silicon surface microroughness on the minority-carrier recombination life-time has been studied with a laser/microwave photoconductance technique. By means of an algorithm for separating the surface and bulk components, it has been shown that the microroughness considerably affects the surface recombination velocity, in turn the lifetime, of silicon wafers at elevated temperatures. It is found that the smoother results in the higher lifetime.

KEYWORDS: microroughness, silicon wafers, lifetime measurement, laser/microwave photoconductance technique, elevated temperatures, surface lifetime

The reduction in surface microroughness of silicon wafers has become more important for the microelectronic device performance and reliability because of the continuous decrease in the device dimension. In fact, it has been reported that the microroughness of silicon wafers greatly affects the electrical properties such as dielectric breakdown integrity of thin oxide films.¹⁻³⁾ In this study, the influence of the microroughness on the minority-carrier recombination lifetime, which is one of the most important electrical properties, has been investigated by means of a noncontact laser/microwave photoconductance (LM-PC) technique.⁴⁻⁶⁾ It is shown that the microroughness considerably affects the lifetime measured at elevated temperatures.

The samples used for this study were single-side polished (100) p-type ($\sim 10 \Omega \cdot \text{cm}$ in resistivity) Czochralski (CZ) silicon wafers. They were sliced from an identical ingot and then prepared by a standard polishing process with variation of the mechanical or chemical components which results in different surface microroughness of polished wafers. The detailed description of the samples is presented in ref. 7, where the samples are classified into four levels denoted as A, B, C, and D in terms of the microroughness as listed in Table I.

Recombination lifetime measurements with the LM-PC technique (LIFETECH-88, SEMITEX Co., Ltd.) were performed in the temperature range from 20°C to 250°C. The decay of excess minority-carriers generated by irradiation with a laser beam ($\lambda = 854 \text{ nm}$) is ob-

served by monitoring the time decay of the microwave (9.6 GHz) reflection power. The laser beam intensity is chosen to satisfy low level excitation conditions. Since the samples were not subjected to any treatment to minimize the surface recombination velocity, the logarithmically transformed carrier decay curve consists of two distinctive regions, i.e., nonlinear initial and linear tail portions. The linear tail portion is used to calculate the effective lifetime (τ_{eff}) defined as $1/\tau_{\text{eff}} = 1/\tau_{\text{surf}} + 1/\tau_{\text{bulk}}$, where τ_{surf} and τ_{bulk} are the surface and bulk lifetime components, respectively. Algorithms for separating the lifetime components have been reported.^{8,9)} In this study, the surface and bulk lifetimes were separately obtained by using the algorithm developed by Buczkowski *et al.*⁹⁾

The effective lifetimes for the four samples with different surface microroughness are shown as a function of temperature in Fig. 1. The difference in the life-

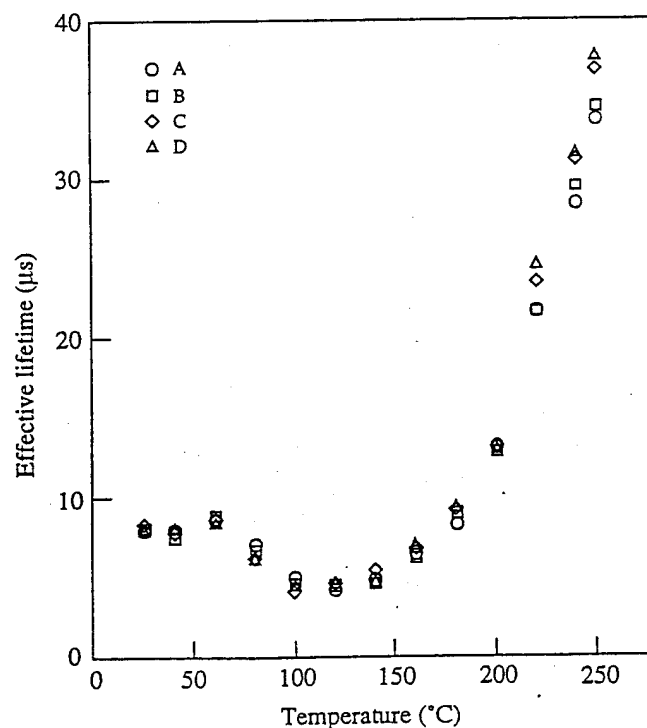


Table I. Microroughness measured by various methods for wafers used in this study.⁷⁾

Wafer	AFM ^{a)} R_a	STYLUS ^{b)} R_a	PSI ^{c)} R_a
A	0.66 nm	0.92 nm	0.72 nm
B	0.51	0.63	0.60
C	0.19	0.20	0.40
D	0.21	0.10	0.30

a) Atomic Force Microscopy.

b) Stylus profilometry.

c) Phase Shift Interferometry.

*On leave from, Showa Denko Silicon K.K., 1505 Shimokagemori, Chichibu, Saitama 369-18.

Fig. 1. Effective lifetime as a function of temperature for wafers with a different surface microroughness level.

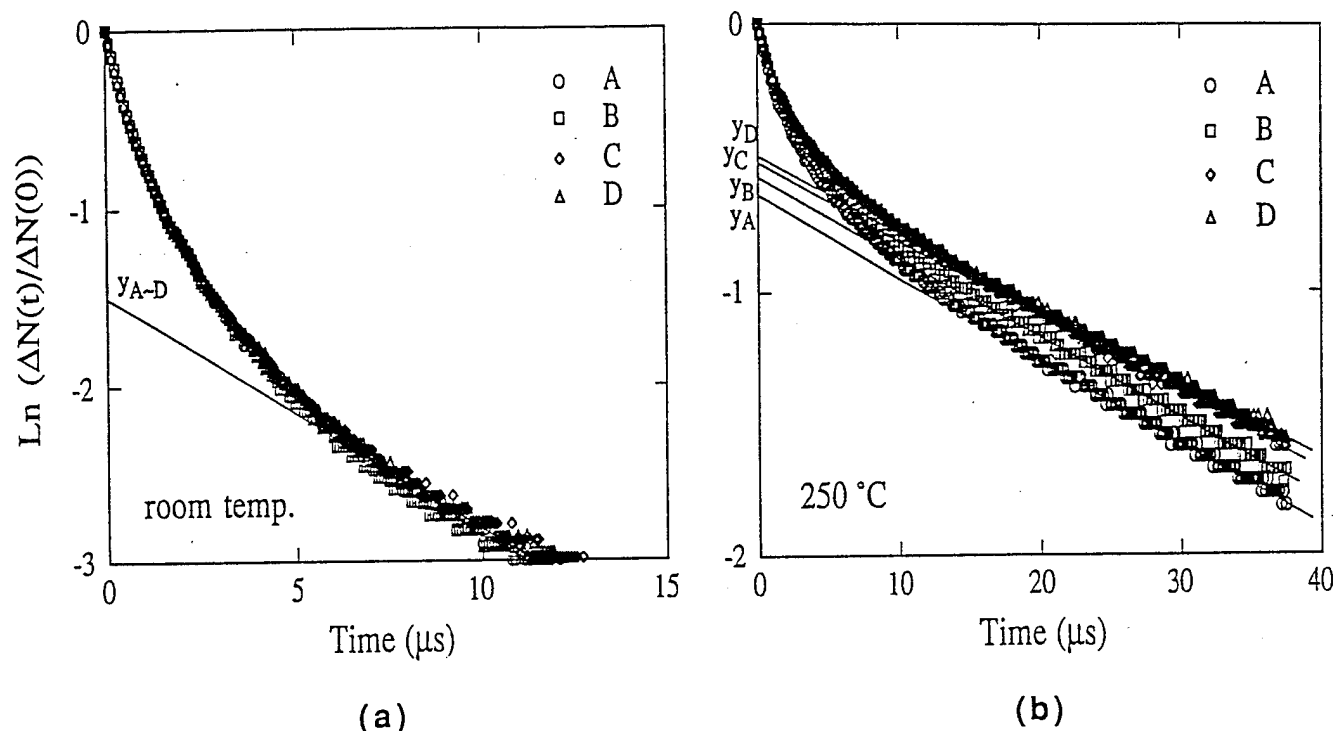


Fig. 2. Carrier decay curves at room temperature and 250°C for wafers with a different surface microroughness level.

time among the samples cannot be observed at temperatures lower than 200°C, whereas, the difference becomes recognizable at higher temperatures. For instance, the sequence of magnitude of the effective lifetime measured at 250°C follows inversely the order of the microroughness, i.e., $\tau_A < \tau_B < \tau_C \leq \tau_D$, although the difference seems to be not very big. However, the corresponding carrier decay curves can be reproducibly distinguished among the samples as shown in Fig. 2 which depicts the typical sets of the decay curves at both room temperature (a) and 250°C (b).

In the literature, it has been reported that the lifetime measured at elevated temperatures is very sensitive to silicon crystal imperfections such as metallic impurities and grown-in defects,^{10,11)} and surface-related defects or states¹²⁾ as well. The surface properties characterized with the microroughness should also contribute to the lifetime of silicon wafers prepared from the same ingot. The y intercepts of the extrapolated lines of the linear part of the decays are indicated in Fig. 2. The y intercept is a factor directly correlated to the surface recombination process which can be derived from the separation factor in the algorithm to separate the surface and bulk lifetime components.⁹⁾ The surface and bulk components, as well as the effective lifetime, obtained by the algorithm are listed in Table II for the samples measured at both the temperatures. It should be emphasized that, although no significant difference in τ_{surf} at room temperature is observed among the samples, they can be clearly distinguished at 250°C. Again the sequence of the magnitude of τ_{surf} is inversely in agreement with the microroughness. Figure 3 clearly depicts the dependence of the surface lifetime on the microroughness.

Table II. Lifetime components after separation procedure measured at room temperature and 250°C.

Wafer	room temperature			250°C		
	τ_{eff} (μs)	τ_{bulk} (μs)	τ_{surf} (μs)	τ_{eff} (μs)	τ_{bulk} (μs)	τ_{surf} (μs)
A	7.9	15.1	16.8	33.6	135.5	46.7
B	8.1	16.0	16.6	34.4	109.3	50.3
C	8.4	16.9	16.7	37.0	130.0	51.6
D	8.0	15.2	16.9	37.7	134.8	52.4

The variation in the bulk lifetime among the samples at 250°C seems not to be significant. This is because of the considerably high inaccuracy of the bulk lifetime determination when the surface lifetime is dominant to the effective lifetime in the employed algorithm. Although all the temperature dependent factors, such as the absorption coefficient and the Fermi energy, should be taken into account for the quantitative analysis, it might be concluded that the surface microroughness of silicon wafers considerably affects the surface recombination lifetime, and in turn the effective lifetime.

It is reasonable to interpret that the reduction in surface roughness results in less interface traps which act as surface recombination centers. In the employed samples, the bulk lifetime obtained at temperatures below 200°C is considerably low, which means that the bulk recombination is a strong contributor to the carrier decay. In consequence, the decay at temperatures below 200°C may not be influenced dominantly by the surface recombination center depending on the microroughness. Whereas, the bulk lifetime becomes

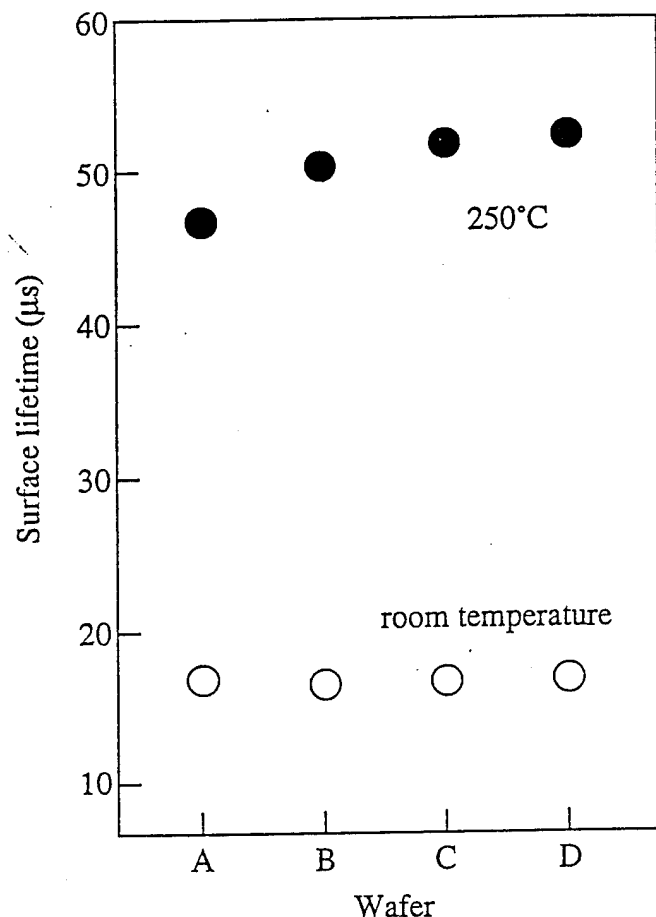


Fig. 3. Dependence of surface lifetime measured at room temperature and 250°C on surface microroughness.

much higher than the surface lifetime at higher temperatures, where the surface recombination is the main

contributor to the decay resulting in the observable dependence on the microroughness.

In summary, silicon wafers with different surface microroughness levels have been studied with recombination lifetime measurements by means of a noncontact LM-PC technique at elevated temperatures. Using the algorithm for the separation of the surface and bulk components, it has been shown that the microroughness considerably affects the surface lifetime of silicon wafers.

The authors are grateful to Dr. Takao Abe (Shinetsu Handotai) for supplying the valuable silicon wafers used in this study.

- 1) T. Abe and M. Kimura: *Semiconductor Silicon 1990*, eds. H. R. Huff, K. G. Barraclough and J. Chikawa (The Electrochemical Society, Pennington, 1990) p. 105.
- 2) M. Morita, A. Teramoto, K. Makiyama, T. Ohmi, Y. Nakazato, A. Uchiyama and T. Abe: *ULSI Science & Technology 1991*, eds. J. Andrews and G. K. Celler (The Electrochemical Society, Pennington, 1991) p. 400.
- 3) T. Ohmi, M. Miyashita, M. Itano, T. Imaoka and I. Kawanabe: *IEEE Trans. Electron Devices* **39** (1992) 537.
- 4) N. J. Harrick: *Solid State Electron.* **27** (1956) 1439.
- 5) H. A. Atwater: *J. Appl. Phys.* **31** (1960) 938.
- 6) R. D. Larrabee: *RCA Rev.* **21** (1960) 124.
- 7) T. Abe, E. F. Steigmeier, W. Hagleiter and A. J. Pidduck: *Jpn. J. Appl. Phys.* **31** (1992) 721.
- 8) A. Usami, S. Jintate and B. Kudo: *Oyo Buturi* **49** (1980) 1192 [in Japanese].
- 9) A. Buczkowski, Z. J. Radzinski, G. A. Rozgonyi and F. Shimura: *J. Appl. Phys.* **72** (1992) 2873.
- 10) F. Shimura, T. Okui and T. Kusama: *J. Appl. Phys.* **67** (1990) 7168.
- 11) Y. Kirino and F. Shimura: *J. Appl. Phys.* **69** (1991) 2700.
- 12) K. Katayama and F. Shimura: *Jpn. J. Appl. Phys.* **32** (1993) L395.

Photoconductance Minority Carrier Lifetime vs. Surface Photovoltage Diffusion Length In Silicon

A. Buczkowski,* G. Rozgonyi,* and F. Shimura*

Department of Materials Science and Engineering, North Carolina State University, Raleigh, North Carolina 27695-7916

K. Mishra*

MEMC Electronics Materials, Incorporated, St. Peters, Missouri 63376

ABSTRACT

Recombination lifetime and diffusion length measured with the photoconductance decay and surface photovoltage techniques are compared theoretically and experimentally, and reasons for possible discrepancies are discussed. Specific examples are given which show that, if full advantage of these noncontact and nondestructive procedures is to be taken, it is necessary that surface recombination be considered in the analysis of any experimental data. This is particularly true for samples where the diffusion length is greater than one-fourth of the wafer thickness, a condition for which it is essential that theoretical algorithms for separating the bulk and surface components of recombination be developed.

Electrical characterization of silicon, especially with those procedures executed in a noncontact fashion, is an important part of material quality evaluation. In the case of high quality silicon wafers electrical probing of the state of charge carriers is the only procedure sensitive enough for defect and impurity observation at low concentrations. Three basic properties of common interest are: (i) minority carrier recombination lifetime, τ , (ii) diffusion length, L ; and (iii) mobility, μ . Actually, these properties are not independent but related via Eq. 7. There are several techniques available for measurement of each of these parameters, among which the photoconductance (PC) decay, surface photovoltage (SPV), and time-of-flight are the most popular for τ , L , and μ , respectively.¹ For silicon with a moderate resistivity mobility values are relatively well established; however, carrier lifetime and diffusion length measurements performed on the same samples can yield significant differences.^{2,3} Thus, it has been noted in Ref. 2 that carrier lifetime methods are "very ambiguous, difficult to interpret, and very unreproducible." Specifically, inconsistent results are often observed when comparing PC lifetime and SPV diffusion length, which violate the expectation justified via Eq. 7. This paper discusses the theoretical basis and potential reasons for these differences using a series of comparative measurements performed with both the SPV and PC techniques on the same samples. It is shown that a much improved data match can be achieved when surface recombination effects are properly accounted for.

Analysis

Photoconductance technique.—In the photoconductance decay technique described here, an excess electron-hole pair concentration is created by an optical-laser illumination. The PC signal is proportional to the number of excess electron-hole pairs integrated over the entire wafer volume. The PC decay is monitored by the change in microwave power reflected from the sample. The carrier transport problem is considered to be one dimensional, since the laser spot size is several times larger than either the wafer thickness or carrier diffusion length. The time dependence of volume integrated density of excess minority carriers can be expressed as a series of exponentially decaying terms

$$N(\alpha_n, t) = A(\alpha_n) \sum_{n=1}^{\infty} B_n(\alpha_n) \exp\left(-\frac{t}{\tau_n}\right) \quad [1a]$$

where

$$B_n(\alpha_n) = \frac{\sin \frac{\alpha_n d}{2} \left[1 - \exp\left(-\frac{T}{\tau_n}\right) \right]}{\frac{1}{\tau_n} (\alpha_n^2 + \alpha_s^2) [\alpha_n d + \sin(\alpha_n d)]} \cdot \left[\alpha_n \sinh\left(\frac{\alpha_n d}{2}\right) \cos\left(\frac{\alpha_n d}{2}\right) + \alpha_n \cosh\left(\frac{\alpha_n d}{2}\right) \sin\left(\frac{\alpha_n d}{2}\right) \right] \quad [1b]$$

A more detailed description of the $A(\alpha_n)$, $B(\alpha_n)$, and τ_n coefficients may be found in Ref. 4 through 7. The absorption coefficient is related to the laser radiation wavelength⁸ by

$$\alpha_n = \left(\frac{85.015}{\lambda} - 77.104 \right)^2 \quad [2]$$

with the wavelength λ in μm and the adsorption coefficient α_n in cm^{-1} .

The series of $\alpha_1, \dots, \alpha_n$ and τ_1, \dots, τ_n coefficients reflect the recombination properties of the sample via hidden parameters like the bulk lifetime τ_{bulk} , surface recombination velocity at the edge of the surface space-charge and bulk regions S , diffusion coefficient D , and wafer thickness d .

The theory of the PC measurements, via Eq. 1a and 1b, indicates that the typically observed nonlinear initial stage of the decay, due to the surface recombination component, becomes linear in its tail portion. From the slope of this linear part of the decay an effective lifetime, τ_{eff} , can be determined. The effective lifetime defined as a reciprocal slope of the tail portion of the decay does not represent the true bulk lifetime but is the sum of two recombination lifetime components, namely, the bulk and the surface lifetime, as given by Eq. 3

$$\frac{1}{\tau_{\text{eff}}} = \frac{1}{\tau_{\text{bulk}}} + \frac{1}{\tau_{\text{surf}}} \quad [3]$$

where

$$\frac{1}{\tau_{\text{surf}}} = \alpha_1^2 D \quad [3a]$$

with α_1 being the first root of

$$\alpha_n d = \arctan\left(\frac{S_1}{\alpha_n D}\right) + \arctan\left(\frac{S_2}{\alpha_n D}\right) + (n-1)\pi \quad [3b]$$

where d is the wafer thickness, D is the carrier diffusion constant, and S_1 and S_2 the front and back surface recombination velocity, respectively.

Actually, the effective lifetime is only a rough measure of material quality, even though it is sensitive to bulk defects and impurities via the bulk lifetime, τ_{bulk} , it also depends on the surface quality, sample thickness, and the carrier mobility through the surface lifetime component τ_{surf} . This de-

* Electrochemical Society Active Member.

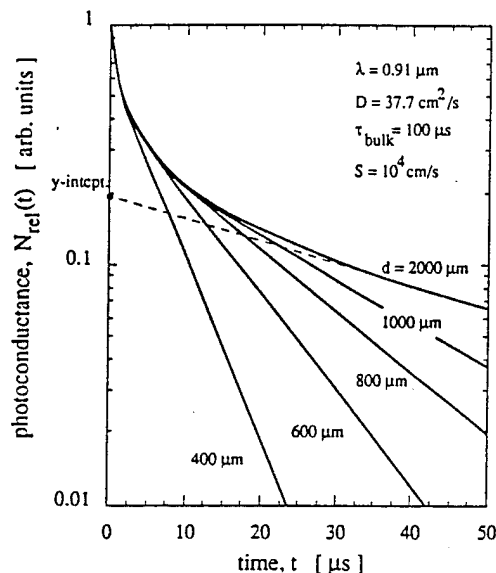


Fig. 1. Theoretical decay profiles of the normalized minority-carrier density for surface recombination velocity $S_1 = S_2 = S = 10^4$ cm/s, diffusion coefficient $D = 37.7$ cm²/s, bulk lifetime $\tau_{\text{bulk}} = 100$ μs, and laser wavelength $\lambda = 0.91$ μm, for wafer thicknesses d from 400 to 2000 μm.

pendence is especially important in currently available high quality silicon characterized with high lifetime/long diffusion length values. Thus, the effective lifetime may be significantly different from the bulk lifetime, especially when samples are relatively "thin" with respect to the diffusion length, i.e., the bulk lifetime is large. An example of the influence of wafer thickness on the shape of a decay profile is illustrated in Fig. 1. Note that as the slope of the tail portion of the decay curve changes, so does the effective lifetime. The magnitude of these wafer thickness-dependent effective lifetime changes can be observed in Fig. 2a

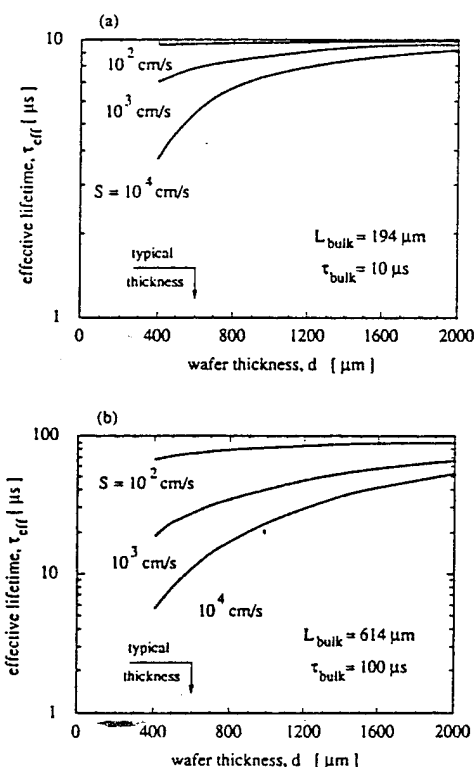


Fig. 2. Influence of wafer thickness d on the effective lifetime observed with the PC technique for surface recombination velocity $S_1 = S_2 = S = 10^4$ cm/s, and bulk lifetimes of (a) 10 and (b) 100 μs.

and b, for 10 and 100 μs bulk lifetimes, respectively, as a function of S . Note that τ_{eff} only asymptotically approaches the bulk value, even though the sample is relatively thick. This is particularly serious for high values of the surface recombination velocity. For example, a sample with a 100 μs bulk lifetime, even if it is 2 mm thick, yields an effective lifetime of only 55 μs, if the surface recombination velocity is of the order of 10^4 cm/s. In this case τ_{eff} is obviously dominated by its surface component, τ_{surf} . Therefore, in order to obtain an accurate measure of the bulk lifetime one must reduce the surface effects, e.g., surface passivation by thermal oxidation is commonly used. A mathematical aid to the separation of surface and bulk components is also possible by proper analysis of the shape of the signal decay which results from the recombination process. For example, as described in Ref. 6, the surface recombination component of lifetime can be determined by extrapolating the tail portion of the carrier decay curve to the carrier axis, as marked by the y intercept point in Fig. 1. Even though the slope of this curve depends on both surface and bulk properties, it was shown in Ref. 6 that for laser pulses much shorter than the measured lifetime the y intercept depends only on the surface component of lifetime. Thus, once τ_{surf} is known, the bulk lifetime can be calculated from Eq. 3. A wide range of surface lifetimes, corresponding to surface recombination velocities from 10^2 to 10^5 cm/s, and bulk lifetimes from a few microseconds to several hundred microseconds, can be determined with an algorithm described.

Surface photovoltage technique.—In the SPV method the diffusion length rather than the recombination lifetime is measured. For this purpose the dependence of surface photovoltage ΔV_s is examined as a function of illumination wavelength or photoabsorption coefficient, which are related to each other as shown in Eq. 2. The measurement is also a noncontact one since the probe is capacitively coupled to the semiconductor. Either no or a very simple sample preparation, e.g., boiling in water, is required since the space-charge region responsible for the photovoltage signal generation exists intrinsically at the silicon surface due to the charge associated with the surface and native oxide defects.⁹⁻¹² Two approaches are commonly applied, either photon flux Φ_{eff} variations due to a change of illumination wavelength, made with the surface photovoltage ΔV_s kept constant, or changes in ΔV_s are recorded for constant Φ_{eff} conditions. Both approaches should lead to the same results for a low illumination intensity when the surface photovoltage is of the order of few millivolts or less, particularly if the surface defect density is relatively high, i.e., at or above 10^{10} cm⁻², depending on the defect capture cross sections and deep energy levels. Three different surface states related to the near surface space-charge region can be considered, they are the surface inversion, depletion, and accumulation, see Ref. 13. The ΔV_s is the highest for the surface strong inversion conditions when for p-type Si it is equal to

$$\Delta V_s = \frac{kT}{q} \frac{p_0}{n_i} \Delta n \quad [4]$$

where kT/q is the thermal potential, Δn the excess carrier concentration at the front surface, and n_i and p_0 the intrinsic and majority carrier concentrations, respectively. For accumulation layer conditions a similar expression can be written

$$\Delta V_s = \frac{kT}{q} \frac{1}{p_0} \Delta n \quad [5]$$

For intermediate depletion layer conditions the ΔV_s will vanish whenever the flatband condition is satisfied, i.e., $V_s = 0$.

The excess carrier concentration, Δn , for low excitation levels is obtained from the solution of the one-dimensional continuity equation, see Eq. 6. It is subject to boundary conditions similar to those for the PC method,^{1,9} however,

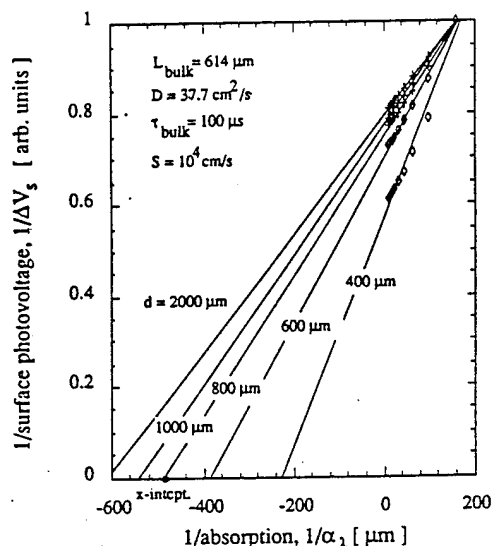


Fig. 3. SPV plots for the same data as in Fig. 1, i.e., $S_1 = S_2 = S = 10^4$ cm/s, diffusion coefficient $D = 37.7$ cm²/s, bulk lifetime $\tau_{\text{bulk}} = 100$ μ s, with wafer thickness as a parameter. Calculation data are marked with different symbols for $d = 400$ to 2000 μ m.

with SPV, steady-state instead of transient conditions must be considered

$$\Delta n = \frac{\Phi_{\text{eff}} \alpha_{\lambda} \tau_{\text{bulk}}}{(\alpha_{\lambda}^2 L_{\text{bulk}}^2 - 1)} \left[\frac{A}{C} + \frac{B}{C} e^{-\alpha_{\lambda} d} - 1 \right] \quad [6]$$

where

$$A = (S_1 S_2 L_{\text{bulk}} / D + S_2 \alpha_{\lambda} L_{\text{bulk}}) \sinh(d / L_{\text{bulk}}) + (S_1 + \alpha_{\lambda} D) \cosh(d / L_{\text{bulk}}) \quad [6a]$$

$$B = (S_2 - \alpha_{\lambda} D) \quad [6b]$$

$$C = (S_1 S_2 L_{\text{bulk}} / D + D / L_{\text{bulk}}) \sinh(d / L_{\text{bulk}}) + (S_1 S_2) \cosh(d / L_{\text{bulk}}) \quad [6c]$$

and L_{bulk} is the bulk diffusion length related to bulk lifetime with the relationship

$$L_{\text{bulk}} = \sqrt{\frac{kT}{q}} \mu \tau_{\text{bulk}} \quad [7]$$

Carrier mobilities of 450 and 1450 cm²/Vs for n- and p-type wafers,¹⁴ respectively, are assumed in our calculations consistent with the resistivity range studied here.

A typical surface photovoltage analysis for the constant Φ_{eff} mode plots the reciprocal of the ΔV_s signal vs. reciprocal absorption coefficient. The data points should yield an approximately linear plot, as presented in Fig. 3 for a number of wafer thicknesses. The data presented in Fig. 3 are based on the same set of parameters used to plot the PC decays presented in Fig. 1. The diffusion length L is obtained from the absolute value of the x intercept point of the straight line. It is evident from the figure that the x intercept varies with the wafer thickness and reaches the true L_{bulk} only if the sample is three to four times thicker than the diffusion length. Thus, it is essential that the diffusion length measured via SPV be called an effective L , similar to τ_{eff} with the PC measurement. It is advantageous to define an effective diffusion length as

$$\Delta V_s^{-1} = C_1 (1/\alpha_{\lambda} + L_{\text{eff}}) \quad [8]$$

where C_1 is a constant of proportionality. L_{eff} is determined using the linear least squares fitting method of theoretically calculated or experimentally measured points to a straight line as marked in Fig. 3. It is important to mention that this definition does not imply that L_{eff} determined via an SPV experiment is related to the τ_{eff} as monitored in the PC technique. In fact, these two "effective" parameters are

derived from very different physical effects and are not related via Eq. 7, which is valid only for true bulk properties.

In order to predict the influence of wafer thickness on the SPV measurement results, the theoretical dependence of effective diffusion length, based on Eq. 8, was calculated and results are presented in Fig. 4. Although the effective SPV diffusion length can have a value lower or higher than the true bulk diffusion length, depending on the specific value of surface recombination velocity, the correct diffusion length is only recovered using wafers that are three to four times thicker than the diffusion length. It has also been observed that the SPV or PC decay curve linear correlation factor R does not bear a first-order relationship with the τ and L fluctuations, since essentially unity R values were obtained in both calculations presented in Fig. 1 and 3. This occurs in spite of the fact that the surface recombination is obviously a part of the total recombination process.

Comparison of PC and SPV theories.—Based on the above theoretical analysis of the influence of wafer thickness on the effective lifetime and effective diffusion length we recognize that before lifetimes/diffusion lengths are compared further discussion of the SPV and PC data analysis is required. For example, we compared first bulk lifetime determined in the PC experiment with its equivalent observed in the SPV. As mentioned, there are several ways to obtain a true bulk lifetime value in the PC experiment. Perhaps the most straightforward is to decrease surface recombination effects by wafer oxidation, but this solution may interfere with the need for a nondestructive measurement. Another is to prepare a specially tailored thick sample. This solution is also most often used for the SPV measurements; however, it is not compatible with using standard thickness wafers with a high throughput capability. For this reason, several algorithms have been developed for separation of the bulk and surface lifetime component based on the shape of the PC decay.⁴⁻⁷ As a result, a full set of four parameters, that is the effective, the bulk, and the surface lifetimes along with the surface recombination velocity can be evaluated. Moreover, the initial nonlinear

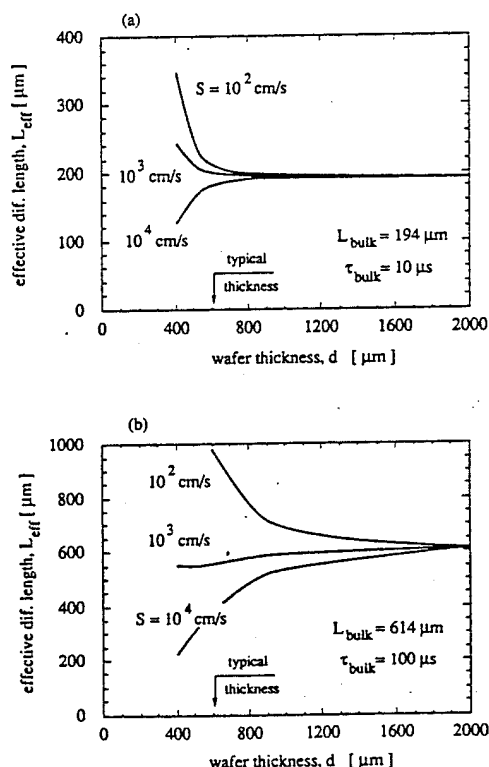


Fig. 4. Influence of wafer thickness d on the effective diffusion length observed with the SPV technique for surface recombination velocity $S_1 = S_2 = S = 10^4$ cm/s, and bulk diffusion lengths of (a) 194 and (b) 614 μ m.

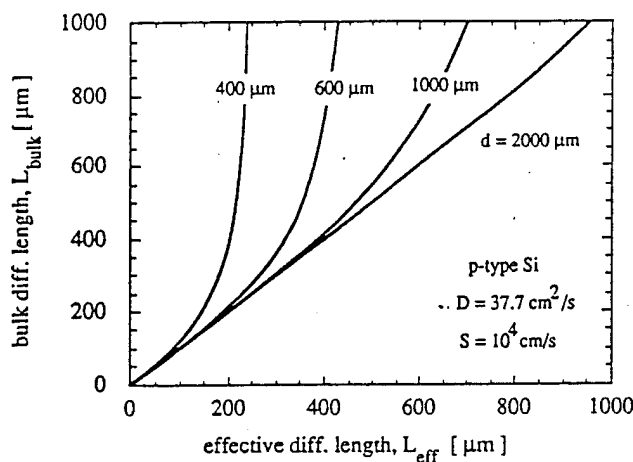


Fig. 5. Theoretical dependence of bulk vs. effective diffusion length with wafer thickness as a parameter for p-type silicon with $S = 10^4 \text{ cm/s}$.

part of the decay is a visual indicator of the importance of the surface component as a part in the overall recombination process. In case of the SPV technique there is no such algorithm available yet for "thin" samples of interest although the problem has already been addressed.¹⁵ For "thick" samples the front surface recombination velocity can be calculated from the y intercept point of the SPV plot. Also, by measuring the saturation value of the ΔV signal at high injection level, it is possible to calculate the surface charge and surface recombination velocity, and to the extent that a distribution of defect/contaminant energy levels and capture cross sections are known the surface concentrations of defect states can be estimated.² If the surface recombination velocity is known then the effective diffusion length measured in the SPV experiment can be corrected (based on the wafer thickness) and the true L_{bulk} determined. Toward this end one can assume identical S values as experimentally determined from the corresponding PC measurement since in both experiments the same bare, untreated silicon samples were used. The bulk diffusion length L_{bulk} is obtained by matching the expected effective diffusion length in Eq. 8 with the experimentally measured L_{eff} . This procedure has been applied in the experiment detailed below. In addition for use as a rough estimate a theoretical plot of bulk diffusion length vs. effective diffusion length with wafer thickness as a parameter is presented in Fig. 5.

Experimental Procedures

Experimental comparative PC vs. SPV tests were performed on several n- and p-type, 6 in. diam, 10 to 20 Ωcm CZ silicon wafers. In the first part of the experiment, several wafers of different thickness were measured. The samples were cut from the same part of an ingot to assure similar bulk properties/lifetimes. In order to observe an influence of surface recombination velocity on effective diffusion length a bare, untreated sample was compared with a sample passivated by immersing in an iodine-based solution during measurements. In the second part of the experiment four samples with a wide range of lifetime values were used. These included an n-type, intentionally thick (2 mm) sample characterized with high lifetime, and three p-type, standard thickness (0.675 mm) wafers of high, medium, and low lifetime. Since the wafers have an intrinsically built-in space-charge region, no special surface preparation was needed. Each sample was measured at several locations with approximately the same repeat pattern using both the SPV and PC techniques. Sample No. 14 was measured before and after annealing at 200°C, as well as following high power light exposure in order to dissociate the Fe-B complex, present in the sample due to a background contamination, into interstitial iron and substitutional boron. This sample is referred as 14R and 14A, for

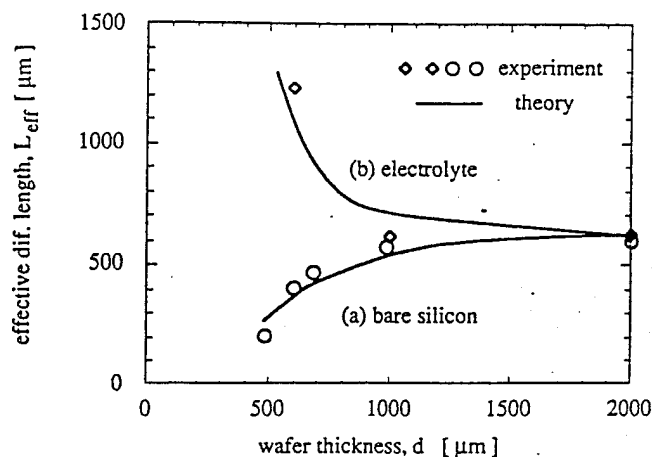


Fig. 6. Effective diffusion length measured for (a) bare and (b) immersed in electrolyte silicon samples of different thicknesses. Theoretical results are also shown assuming surface recombination velocity $2 \cdot 10^4 \text{ cm/s}$ and 20 cm/s , for (a) and (b), respectively.

the reference and annealed data, respectively. In this way one sample functioned as both a medium and low lifetime sample, since Fe is essentially much less active as a recombination center when it resides within a Fe-B complex, but becomes a very active deep level after thermal or optical dissociation. Since the dissociation process is reversible with a time constant of several days at room temperature, it was possible for the SPV and PC measurements to be carried out separately and then cross examined. For the PC measurements a noncontact laser excitation/microwave reflection system, Lifetech-88[®] (SEMITECH Company Limited, Japan),¹⁶ operating with a laser wavelength 910 nm and pulse width of 150 ns was used. SPV measurements were performed on the noncontact, capacitively coupled, CMSIII[®] (Semiconductor Diagnostics, USA)² system using a white spectrum lamp with monochromatic light excitation cut off via 1.0, 0.975, 0.950, 0.925, 0.900, 0.850, and 0.800 μm narrow band filters. The constant photon flux mode of operation was applied.

Experimental Results

The influence of wafer thickness on SPV-measured diffusion lengths for wafers characterized with two significantly different surface conditions is presented in Fig. 6. The results of theoretical calculations are also shown for comparison. Typical surface recombination velocity values equal to $2 \cdot 10^4 \text{ cm/s}$ and 20 cm/s were assumed for this purpose for the bare and chemically passivated surfaces, respectively. In spite of the accuracy of theoretical and experimental data matching, which seems reasonable in

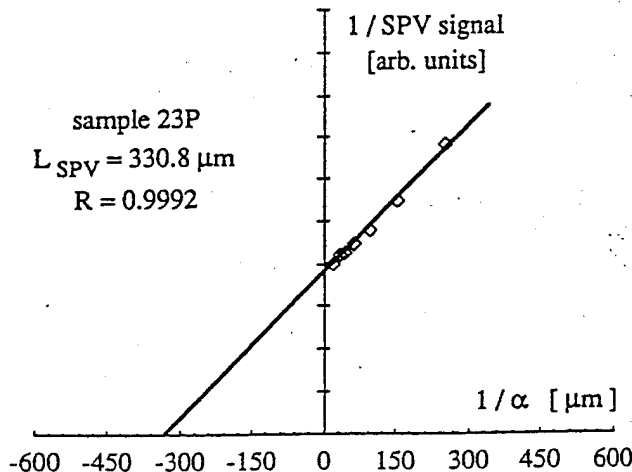


Fig. 7. Typical experimental SPV plot for the 23P sample.

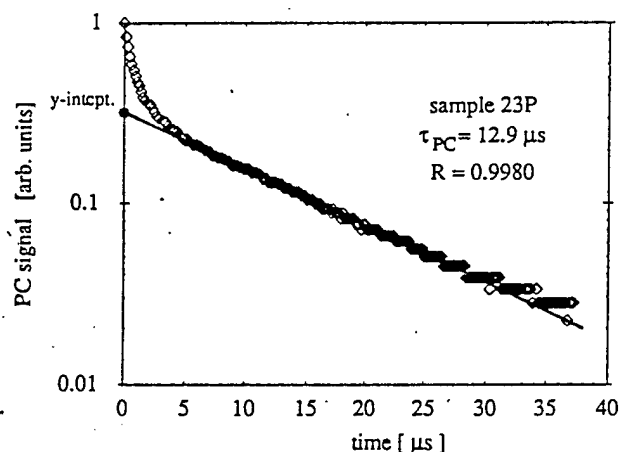


Fig. 8. Typical experimental PC decay for the 23P sample.

Fig. 6, it is evident that wafer thickness must be taken into account for a correct evaluation of diffusion length in "thin" samples. Moreover, an analysis procedure which is able to determine the surface recombination velocity at the back side of wafer must be derived before the true diffusion length can be recovered. To the best of our knowledge, such a procedure is not yet available; therefore, in subsequent experimental SPV data analyses, the surface recombination velocities measured with the PC technique were assumed.

A typical surface photovoltage analysis for each of the seven narrow band filters yields an approximately linear plot, as presented in Fig. 7 for sample No. 23P. The diffusion length, L_{eff} , is obtained from the absolute value of the x -intercept point of the straight line. Note that the linear ΔV_s^{-1} vs. α_A^{-1} correlation factor is $R = 0.9992$ in Fig. 7 and was close to unity for every case studied. The corresponding "raw" photoconductance decay data for the same sample are shown in Fig. 8. The nonlinear initial part of the decay due to the surface recombination component, becomes linear in its tail portion, as expected. For both the SPV and PC measurements the measurement error of the same point was on the order of few percent, while the wafer uniformity was better than 10%. The experimental L_{eff} by SPV and τ_{eff} by PC data and calculated complementary value for τ_{SPV} and L_{PC} , based on Eq. 7, are summarized in Table I along with other sample data.

Table I. Sample descriptions and initial "raw" measurement results.

Sample	Type	Thickness (μm)	L_{eff} (μm)	$L_{PC}^{(c)}$ (μm)	$\tau_{SPV}^{(c)}$ (μs)	τ_{eff} (μs)	Difference in τ (%)
23P	p-Type	675	331	220	29.1	12.8	± 39
MER	p-Type	675	396	231	41.6	14.2	± 49
14R ^(a)	p-Type	675	302	214	24.2	12.2	± 33
14A ^(b)	p-Type	675	144	144	5.5	5.5	0
37N	n-Type	2000	654	560	366	268	± 16

^a Measured before Fe-B pair dissociation.

^b Same sample as 14R but after Fe-B pair dissociation.

^c Obtained with Eq. 7.

Table II. Measurement results for the PC technique after lifetime component separation.

Sample	τ_{eff} (μs)	τ_{bulk} (μs)	τ_{surf} (μs)	$S \cdot 10^4$ (cm/s)	L_{bulk}^* (μm)
23P	12.8	40.9	18.8	1.2	393
MER	14.2	57.7	19.2	1.1	466
14R	12.2	34.3	19.1	1.1	360
14A	5.5	7.1	24.5	0.41	164
37N	268	420	647	0.03	701

* Based on τ_{bulk} and Eq. 7.

Table III. Bulk diffusion length calculations based on the effective diffusion lengths listed in Table I and surface recombination velocity from Table II.

Sample	L_{eff} (μm)	τ_{eff} (μs)	L_{bulk} (μm)	τ_{bulk} (μs)	$S \cdot 10^4$ (cm/s)
23P	331	29.1	377	37.8	1.2
MER	396	41.6	514	70.1	1.1
14R	302	24.2	331	29.1	1.1
14A	144	5.5	144	5.5	0.41
37N	654	366	655	367	0.03

It is evident that the PC results are consistently lower than the SPV data with the exception of sample 14A, where an excellent agreement was reached. However, the τ_{SPV} and L_{PC} are included in Table I only as a means of "early" comparison; since prior results from the theory of SPV and PC measurements do not justify using Eq. 7 for the effective values. Therefore, the true bulk lifetime was determined from the initial PC measurement results by applying the PC separation algorithm as summarized in Table II.

Again, there is no satisfactory agreement reached yet between the bulk PC diffusion length obtained after the separation procedure, and the SPV data in Table I. However, now the PC L_{bulk} is consistently longer than the SPV L_{eff} , and it is reasonable to suspect that the SPV results are, in fact, also dependent on the surface recombination process. Actually, a surface influence for SPV is very likely, since the PC technique uses one of the same illumination wavelengths as the SPV measurement. Since the simplified SPV theory allows the use of Eq. 8 only if the diffusion length is approximately one-fourth of the wafer thickness,¹ then L_{eff} reaches L_{bulk} as illustrated in Fig. 4. This condition is only fulfilled in Table I for sample No. 14A where the dissociated Fe in the annealed sample has reduced the diffusion length to 144 μm , which happens to be about one-fourth of the wafer thickness. Thus, all untreated samples must be considered to be relatively "thin." For this reason the bulk values of the SPV diffusion length were estimated by taking the experimental effective diffusion length and assuming surface recombination velocity as determined in the PC experiment. The results using this approach for bulk SPV lifetime estimations are summarized in Table III.

Generally the SPV L_{bulk} values are longer than the effective ones, similar to the PC bulk lifetimes which were longer than the effective lifetimes. Finally, the actual PC and SPV diffusion length/recombination lifetime specified in the Tables II and III have been collected in Table IV where it can be seen that a much better agreement than initially presented in Table I is reached.

Conclusions

The recombination lifetime and diffusion length measured with the surface photovoltage and photoconductance technique were compared for a variety of silicon, n- and p-type samples. Initially, significant "raw" data discrepancies of the order of 50% were observed between two techniques when applied to the same samples. These discrepancies result from the influence of the surface recombination component affecting the measurements to a different degree for each technique. The correct analysis has to include the lifetime component separation in order to determine the true bulk properties, especially in high quality

Table IV. Final comparison of the bulk diffusion lengths and lifetimes determined in SPV and PC measurements after eliminating the surface recombination effects.

Sample	L_{SPV} (μm)	L_{PC} (μm)	τ_{SPV} (μs)	τ_{PC} (μs)	Difference in τ (%)
23P	517	393	37.8	40.9	± 4
MER	514	466	70.1	57.7	± 10
14R	331	360	29.1	34.3	± 8
14A	144	164	5.5	7.1	± 12
37N	655	701	367	420	± 7

materials where the samples are relatively "thin" with respect to the diffusion length. To this end several separation algorithms are available for the PC technique, whereas they await future development for the SPV technique. It is shown that both techniques can lead to an agreement within 15%, if the influence of surface recombination effects is eliminated and the bulk lifetimes are compared.

Acknowledgments

This work has been supported by the National Renewable Energy Laboratory.

Manuscript submitted April 12, 1993; revised manuscript received July 19, 1993.

North Carolina State University assisted in meeting the publication costs of this article.

REFERENCES

1. D. K. Schroder, *Semiconductor Material and Device Characterization*, pp. 194-243, 359-448, John Wiley & Sons Inc., New York (1990).
2. J. Lagowski, P. Edelman, M. Dexter, and W. Henley, *Semicond. Sci. Technol.*, **7**, A185 (1992).
3. L. Coates, O. Anttila, C. Kung, L. Caubin, J. Thomas and S. Hahn, Abstract 874, p. 1288, The Electrochemical Society Extended Abstracts, Vol. 93-1, Honolulu, HI, meeting, May 16-21, 1993.
4. K. Luke and L. Cheng, *J. Appl. Phys.*, **61**, 2282 (1987).
5. A. Buczkowski, Z. Radzinski, G. Rozgonyi, and F. Shimura, *J. Appl. Phys.*, **69**, 6495 (1991).
6. G. Kousik, Z. Ling, and P. Ajmera, *ibid.*, **72**, 141 (1992).
7. A. Buczkowski, Z. Radzinski, G. Rozgonyi, and F. Shimura, *ibid.*, **72**, 2873 (1992).
8. M. Saritas and H. McKell, *ibid.*, **63**, 4561 (1988).
9. D. Fitzgerald and A. Grove, *Surf. Sci.*, **9**, 347 (1968).
10. A. Many, Y. Goldstein, and N. B. Grover, *Semiconductor Surfaces*, p. 128, North-Holland Publ. Co., Amsterdam (1965).
11. F. Bertz, in *Surface Physics of Phosphors and Semiconductors*, C. G. Scott and C. E. Reed, Editors, p. 143, Academic Press, Ltd., London (1975).
12. A. Buczkowski, G. Rozgonyi, and F. Shimura, *Jpn. J. Appl. Phys.*, **32**, L218 (1993).
13. E. Johnson, *J. Appl. Phys.*, **23**, 1349 (1957).
14. For example, N. Arora, J. Hauser, and D. Roulston, *IEEE Trans. Electron Devices*, **ED-29**, 292 (1982).
15. O. Anttila and S. Hahn, *This Journal*, **139**, (6), 309C (1992).
16. F. Shimura, T. Okui, and T. Kusama, *J. Appl. Phys.*, **67**, 7168 (1990).

Separation of the bulk and surface components of recombination lifetime obtained with a single laser/microwave photoconductance technique

A. Buczkowski, Z. J. Radzinski, G. A. Rozgonyi, and F. Shimura
Department of Materials Science and Engineering, North Carolina State University, Raleigh,
North Carolina 27695-7916

(Received 27 September 1991; accepted for publication 8 June 1992)

An algorithm for separating the bulk and surface components of recombination lifetime obtained via a contactless *single* laser excitation/microwave reflection decay measurement is presented. The surface recombination component of lifetime is determined by extrapolating the tail portion of the carrier decay curve to the carrier axis. Although the slope of this curve depends on both surface and bulk properties, it is shown that the y intercept depends only on the surface component of lifetime. A wide range of surface lifetimes, corresponding to surface recombination velocities from 10^2 to 10^5 cm/s, and bulk lifetimes from a few microseconds to several hundred microseconds can be measured. An experimental verification of the analysis is presented using microwave absorption/reflection measurements on silicon wafers representing a wide variety of bulk and surface lifetime components.

INTRODUCTION

Minority carrier recombination lifetime is a basic electrical property of semiconductors and provides important information about material quality. For its measurement, contactless, nondestructive, and high throughput techniques are especially desired. The laser excitation/microwave reflection photoconductance (LM-PC) method meets many of these basic requirements. However, the correct interpretation of LM-PC decay curves requires a detailed understanding of the origin of carrier recombination processes, and special attention must be paid to the separation of different components of recombination lifetime. It is commonly recognized that recombination effects in silicon crystals are mainly attributed to the presence of defects located within the forbidden gap which act as recombination centers (traps). With respect to the volume distribution of these defects, two distinct regions must be considered: the bulk of the wafer which generally has a relatively low density of defects, and the more highly defected (or contaminated) near-surface region. Generally, an "effective" lifetime, having two components, designated bulk and surface, is specified for a given wafer. The bulk component is controlled by the concentration N_T of recombination centers, their capture cross section σ , and their energy levels E_T ; whereas the surface component depends on surface recombination velocities, S_{front} and S_{back} , carrier diffusion constant D , and wafer thickness d .^{1,2} It should be noted that although the diffusion constant and wafer thickness control the surface lifetime component they are actually bulk and not surface properties.

In high quality materials the bulk lifetime, τ_{bulk} can be much longer than the surface lifetime, τ_{surf} which on the bare silicon is usually in the order of tens of microseconds. As a result the measured "effective" lifetime τ_{eff} is dominated by its surface component. Therefore, in order to obtain the bulk lifetime, a separation of two components is obligatory or, as a possible solution of the problem, those practical situations for which the surface component is

negligible must be verified. For example, this happens when either the carrier diffusion constant or surface recombination velocities are small, or the measured wafer is thick. In these cases, the surface recombination process is limited either by the low flux of carriers diffusing toward the surface, by the low surface recombination velocity itself, or if the ratio of carriers recombining at the surface to that within the bulk is low due to the large thickness of the measured wafer. All of these possibilities are observed in practice. In low quality material, the effective lifetime is assumed to be equal to the bulk, due to the low diffusion coefficient. Otherwise, a wafer of significantly larger thickness, sometimes up to 1 cm, has to be prepared for measurements.^{1,3} It is also possible to reduce the surface recombination velocity either by oxidation,⁴ or by chemical immersion during measurement.⁵ It has also been noticed that the surface activity can be changed by wafer irradiation with ultraviolet light,⁶ although in this case the surface activity is not constant with time and the physical mechanism is not yet fully understood. For all of these cases, the surface recombination component is negligible and the measured effective lifetime may be assumed to be equal to the bulk.

Unfortunately, these limiting cases are not always applicable. They require a special sample preparation when a thick wafer without any reference to the actual size is used, or are destructive and time consuming since the oxidation process may change the initial lifetime value. Moreover, they may be limited for some applications, e.g., immersing in chemicals for measurements at temperature elevated up to 250 °C. The separation of surface and bulk components is also possible by an analysis of the shape of the signal decay which results from recombination processes.^{7,8} Recently, a new algorithm has been presented⁹ for separating the bulk and surface components of recombination lifetime, which is based on two measurements of the sample excited consecutively by two lasers of different wavelengths. The difference in shape of the two corresponding decay curves, which results from a geometrical change in

the electron-hole pair generation function, was evaluated to yield the surface recombination velocity. In this article an improved algorithm which is applicable for analysis of data obtained with one laser only is presented. Although the elimination of one of the two excitation lasers was achieved, the measurement concept for the separation remains essentially the same. In this way a significant simplification of the system with a decrease in measurement time and enhanced accuracy was achieved. This report presents an experimental verification of the new single laser approach, and discusses practical aspects of the technique in terms of its limits and accuracy.

ANALYSIS

In the laser/microwave photoconductance technique described here, the excess electron-hole pair concentration created by an optical-laser illumination is monitored via the reflectance of a microwave beam probing the sample. At the applied oscillator frequency of 9.6 GHz for a wafer resistivity above 1 Ω cm, the microwave penetration depth is typically larger than the wafer thickness. Therefore, the signal decay is proportional to the number of excess electron-hole pairs integrated over the entire wafer volume. The carrier transport problem is considered to be one dimensional, since the laser spot size is several times larger than either the wafer thickness or carrier diffusion length. The time dependence of volume integrated density of excess minority carriers can be expressed as a series of exponentially decaying terms:

$$N(\alpha_\lambda, t) = A(\alpha_\lambda) \sum_{n=1}^{\infty} B_n(\alpha_\lambda) \exp\left(-\frac{t}{\tau_n}\right), \quad (1a)$$

where

$$B_n(\alpha_\lambda) = \frac{\sin(\alpha_n d/2) [1 - \exp(-T/\tau_n)]}{(1/\tau_n)(\alpha_n^2 + \alpha_\lambda^2) [\alpha_n d + \sin(\alpha_n d)]} \\ \times [\alpha_\lambda \sinh(\alpha_\lambda d/2) \cos(\alpha_n d/2) \\ + \alpha_n \cosh(\alpha_\lambda d/2) \sin(\alpha_n d/2)]. \quad (1b)$$

A more detailed description of the $A(\alpha_\lambda)$, $B(\alpha_\lambda)$, and τ_n coefficients may be found in Refs. 7 and 9. The series of $\alpha_1, \dots, \alpha_n$ and τ_1, \dots, τ_n coefficients reflect the recombination properties of the sample via hidden parameters like the bulk lifetime τ_{bulk} , surface recombination velocity S , diffusion coefficient D , and wafer thickness d . The separation of bulk and surface components takes advantage of the influence of laser wavelength on the decay profile given by Eq. (1). Since the laser wavelength λ is strictly related to the photoabsorption coefficient α_λ , either factor can be equivalently considered. In this article absorption coefficient rather than laser wavelength is appropriate. A representative family of decay curves with absorption coefficient as a parameter is presented in Fig. 1. Notice that the slope of the curves varies with time, especially for the initial part of the decay, and that these variations are strongly affected by the photoabsorption coefficient. As previously shown,⁷ the slope change can be correlated with the surface recombination phenomenon. For the later part of the decay curves

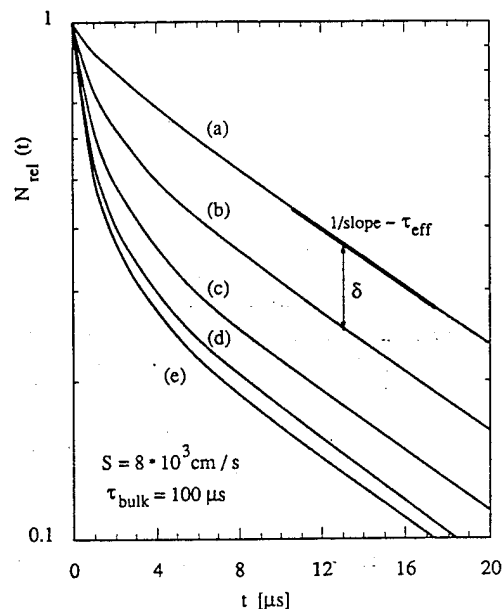


FIG. 1. Decay profiles of the normalized minority-carrier density for wafer thickness $d=650$ μm , diffusion coefficient $D=30$ cm^2/s , and α_λ : λ , i.e., photoabsorption coefficient: wavelength values equal to (a) 12.4 cm^{-1} : 1.06 μm (b) 119.6 cm^{-1} : 0.97 μm , (c) 278.7 cm^{-1} : 0.91 μm , (d) 658.9 cm^{-1} : 0.83 μm , and (e) 1572.5 cm^{-1} : 0.73 μm . The separation is denoted by δ and the effective lifetime by τ_{eff} .

the slope stabilizes at a constant value independent of which absorption coefficient is taken.⁹ This slope is often used to calculate an effective lifetime, sometimes “mathematically” referred to as an asymptotic instantaneous lifetime. Additionally, for each pair of absorption coefficients $\alpha_{\lambda 1}$ and $\alpha_{\lambda 2}$, a separation between decays is observed as a function of time,⁹ see Fig. 1. This separation reaches its limit δ^* when $t \rightarrow \infty$, and in subsequent discussion is called the separation factor:

$$\delta^* = \ln \frac{B_1(\alpha_{\lambda 1}) \sum_{n=1}^{\infty} B_n(\alpha_{\lambda 2})}{B_1(\alpha_{\lambda 2}) \sum_{n=1}^{\infty} B_n(\alpha_{\lambda 1})}. \quad (2)$$

In general, several microseconds are usually long enough to fulfill this condition for a large range of recombination velocities. In the algorithm presented in Ref. 9, the separation factor corresponding to two different photoabsorption coefficients was used to determine the surface recombination effect. This factor is easy to experimentally determine, as will be shown in Fig. 2. δ^* does not depend on τ_{bulk} but is directly related to τ_{surf} which enables us to experimentally determine the surface recombination component, and then use Eq. (3) to calculate the bulk lifetime:

$$\frac{1}{\tau_{\text{bulk}}} = \frac{1}{\tau_{\text{eff}}} - \frac{1}{\tau_{\text{surf}}}. \quad (3)$$

A disadvantage of the algorithm used in Ref. 9 is the necessity of making two consecutive measurements with two different laser wavelengths. However, a detailed study of the separation factor δ^* reveals that it has a finite limit when one absorption coefficient approaches zero. This limit is designated δ_a and is given by the following equation:

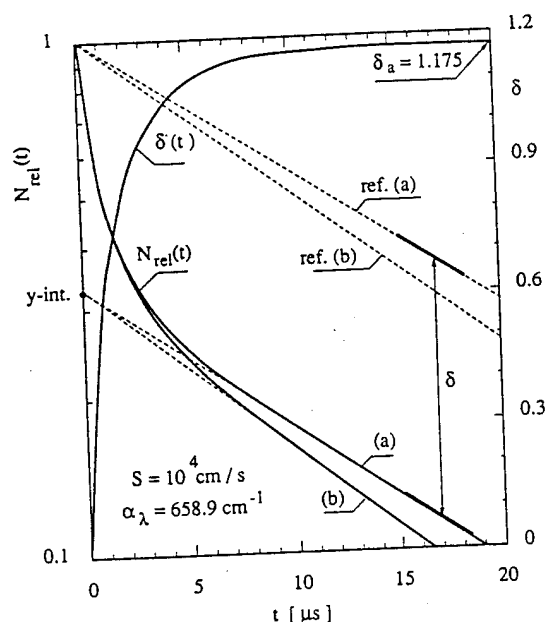


FIG. 2. Simulated decay profiles and separation function δ for wafer with the same value of surface recombination velocity and bulk lifetimes equal to (a) 1000 μs and (b) 100 μs . The y intercept point, the value of separation factor and the reference decays are indicated in the figure.

$$\delta^*(\alpha_{\lambda 2} \rightarrow 0) = \delta_a = \text{const} + \ln \left(B_1(\alpha_{\lambda 1}) / \sum_{n=1}^{\infty} B_n(\alpha_{\lambda 1}) \right). \quad (4)$$

Note that δ_a is a function of only one absorption coefficient (laser wavelength). Additionally, if light with zero absorption coefficient could be used, the corresponding decay would have a slope which is time independent and equal to the effective lifetime. Such a decay is called a reference decay in the following discussion. It can be drawn as a straight line crossing the maximum point of the experimental decay and being parallel to its later part, as presented in Fig. 2. In this figure two decays are simulated, each with a different value of the bulk but the same surface lifetime and the corresponding reference decays are marked. The separation function δ which does not depend on the bulk lifetime is shown, and the value of separation factor δ_a is marked as well. Notice that mathematically this value is an equivalent to the logarithm of y intercept [$\delta_a = \ln(y \text{ intercept})$] of the line, which is an extension of the linear (tail) part of the decay whose the slope defines the effective lifetime. Since identical values of the surface lifetime component are simulated in the figure, both decay curves (a) and (b) extrapolate to the same y intercept, as marked in Fig. 2. Use of this formalism permits, with a single measurement (with one laser wavelength), the experimental δ_{exp} value to be determined and through it, the surface lifetime. To facilitate this analysis the theoretical relations of Eq. (4) above and Eq. (1e) in Ref. 9 have been numerically calculated to specify the separation factor and surface lifetime as a function of the surface recombination velocity which acts as the independent variable. These relations tie the separation factor δ_a with surface recombination velocity,

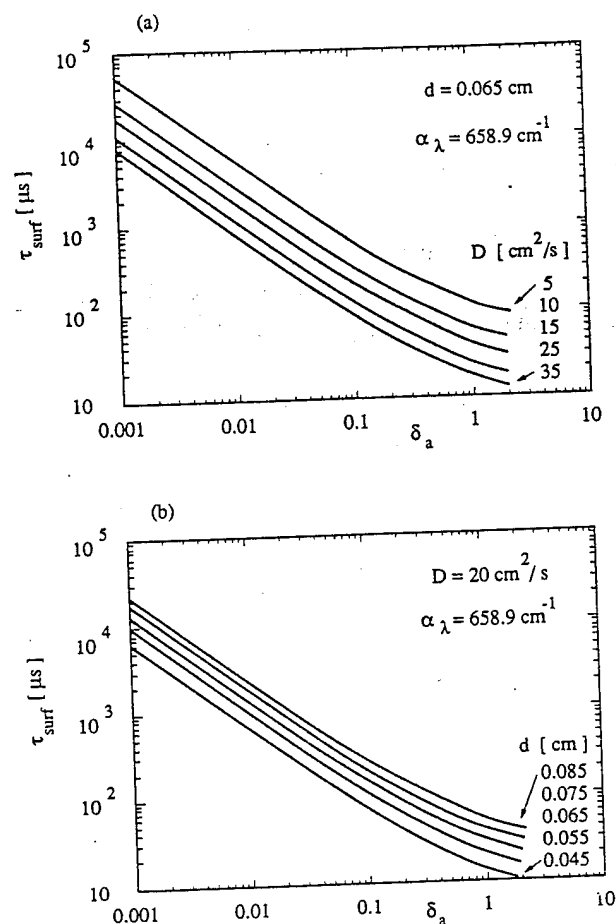


FIG. 3. Relationship of surface lifetime τ_{surf} vs separation factor δ_a with (a) diffusion constant D and (b) wafer thickness d as a parameter.

ity, or finally with the surface lifetime τ_{surf} when surface recombination velocity is eliminated. Following a formal x - y coordinate exchange, the surface lifetime is plotted in Figs. 3(a) and 3(b) as a function of δ_a , with diffusion coefficient D and wafer thickness d used as parameters, respectively. It is clear that for any specific value of the separation factor, the surface lifetime can vary as much as an order of magnitude when the diffusion constant ranges from 5 to 35 cm^2/s (e.g., at room temperature, mobility varies from 192 to 1346 $\text{cm}^2/\text{V s}$). A similar influence of wafer thickness on the surface lifetime is observed, as shown in Fig. 3(b). Therefore, it is essential that the wafer thickness and diffusion constant values are known for the τ_{surf} calculations. Although the geometrical factor d (wafer thickness) can be easily determined, the diffusion coefficient D which is related to carrier mobility μ with relationship $D = \mu kT/q$ always remains uncertain, unless it is measured in a separate experiment. The mobility dependence is often overlooked or ignored, and in practice a reasonable D value is used for calculations without any independent measurements. Unfortunately, any error in the D estimation will be reflected in the τ_{surf} determination and ultimately in the τ_{bulk} evaluation, as will be discussed in next section.

MEASUREMENTS LIMIT: THEORETICAL MODELING

Measurement limits and accuracy are important practical aspects of the τ_{surf} and τ_{bulk} determination. These limits are not only controlled by the accuracy of a specific measurement system itself, but also result from the theoretical formula given by Eq. (3). Noise in the microwave detection/amplification unit and data digitization in analog/digital (A/D) converter are two of the most important sources of measurement error affecting the experimental value of τ_{eff} and δ_a . In order to observe the influence of these error sources on measurement accuracy, a signal decay was simulated assuming an 8 bit A/D converter (256 levels) and signal to noise ratio equal to 100:1. Representative examples of digitized "noisy" decay curves for 10 μs to 1000 μs bulk lifetimes, and a selected decay at 100 μs with its corresponding separation function δ versus time are shown in Figs. 4(a) and 4(b), respectively. By comparison of theoretical initial input data to data extracted back from the decays after digitization using the best linear fitting method, the measurement accuracy is estimated to be within the range of 5–10% for both τ_{eff} and δ_a . Moreover, the error for τ_{surf} obtained from δ_a is also affected by the uncertainty in d and D . If D is not measured, but only "reasonable" value taken into account, the accuracy can be very poor. The error in bulk lifetime τ_{bulk} is larger than for τ_{eff} and δ_a , and depends strongly on how close the τ_{surf} is to τ_{eff} . The expression which describes the accuracy of τ_{bulk} measurement results directly from Eq. (3) and is given by

$$\frac{d\tau_{\text{bulk}}}{\tau_{\text{bulk}}} = \frac{d\tau_{\text{eff}}}{\tau_{\text{eff}}} + \frac{d\tau_{\text{surf}}}{\tau_{\text{surf}}} + \frac{d\tau_{\text{eff}} - d\tau_{\text{surf}}\tau_{\text{surf}}/\tau_{\text{eff}}}{\tau_{\text{surf}}/\tau_{\text{eff}} - 1}. \quad (5)$$

A graphical representation of this equation is presented in Fig. 5; where finite increments $\Delta\tau_{\text{eff}}$ and $\Delta\tau_{\text{surf}}$ were used for the calculations. The highest accuracy of $\Delta\tau_{\text{bulk}}$ which is close to $\Delta\tau_{\text{eff}}$ (assumed to be 5% in Fig. 5) can only be reached when $\tau_{\text{surf}} \gg \tau_{\text{eff}}$. Whereas τ_{surf} is very close to τ_{eff} , e.g., the bulk lifetime is much longer than the surface, the bulk lifetime is extracted with an enormous error and sometimes, in extreme case, it appears to be negative. Such case is not shown in Fig. 5 but it can likely happen when the $\tau_{\text{surf}} < \tau_{\text{eff}}$ due to measurement errors if the τ_{surf} is under and the τ_{eff} overestimated. Most often it results from the overestimated value of the diffusion constant D , which if corrected can partially solve the problem. It is apparent that careful attention must be paid to the data analysis. For example, assuming that an acceptable inaccuracy of $\Delta\tau_{\text{bulk}}$ could be as high as 100% and the inaccuracy of $\Delta\tau_{\text{surf}}$ the same as for $\Delta\tau_{\text{eff}}$ (5%), Fig. 5 predicts that the surface lifetime cannot be less than $1.1\tau_{\text{eff}}$. In other words, an experimental value of the bulk component can be obtained with reasonable error only when the value of measured surface lifetime is more than 10% higher than the effective lifetime.

EXPERIMENTAL RESULTS

An experimental test of the proposed algorithm and estimate the actual values of bulk lifetime measured on

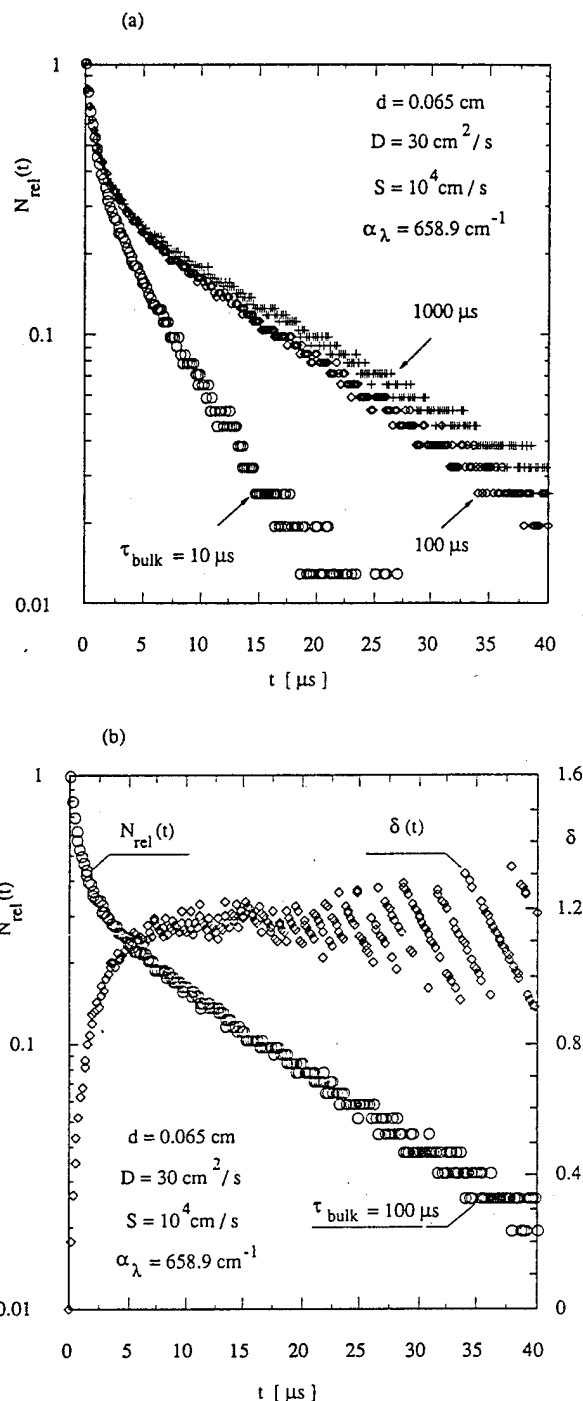


FIG. 4. Simulated "noisy" decays after digitization procedure with (a) bulk lifetime as a parameter and (b) selected corresponding separation function.

bare silicon wafers was performed on four *n*-type, 6-in.-diam, 10 Ω cm CZ silicon wafers with bulk lifetimes which ranged from 3 ms to 1 μs . The wafers were initially oxidized at 1100 $^{\circ}\text{C}$ for 4 h to reduce the surface recombination to a negligible level, i.e., on the order of 0.1 to 1 cm/s. Taking into account that $\tau_{\text{surf}} = 0.5 d/S$, for $S \rightarrow 0$,^{1,2} these recombination velocities correspond to surface lifetime values from 350 to 35 ms, and since $\tau_{\text{surf}} \gg \tau_{\text{eff}}$, Eq. (3) predicts that the bulk lifetime is close to the effective lifetime, when

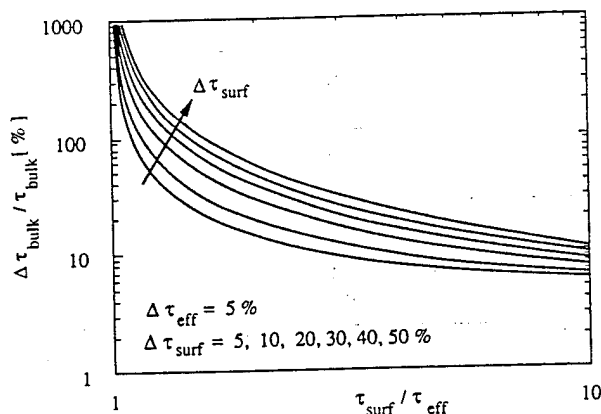


FIG. 5. Inaccuracy of the bulk lifetime determination as a function of ratio of surface lifetime to effective lifetime with inaccuracy of surface lifetime as a parameter.

it is measured on oxidized wafers. The bulk lifetime was then changed by applying different post-oxidation thermal treatments, which introduced a varying number of bulk recombination centers related to oxygen and carbon point defects, precipitates, and dislocation loops.¹⁰ Each sample was measured five times, at the center and at the corners of a 2 cm square. Measurements were performed on each sample four times: following post-oxidation treatment, and then $\frac{1}{2}$, 24, and 200 h after oxide stripping. In this way, the four samples, each with four different values of τ_{surf} but the same of τ_{bulk} were studied. Between measurements the wafers were stored in an air ambient. The measurements were performed on the Lifetech-88[®] system (SEMITECH Co., Ltd.)¹¹ operating with a laser wavelength $\lambda = 830$ nm ($\alpha_{\lambda} = 658.9$ cm⁻¹) and pulse width 150 ns.

Figure 6 shows the influence of time dependent changes in surface condition on photoconductance decay for sample D16. The theoretical decays shown as solid lines, were simulated using $\tau_{\text{bulk}} = 145$ μs and the $\tau_{\text{surf}} = 29.5, 32.7, 37.3$, and $35\,000$ μs , and match the experimental data points quite well. It is clearly seen that the surface recombination activity, most likely related to surface contamination level, strongly affects the measured effective lifetime. An analogous family of experimental data is presented in Fig. 7 for a set of samples which had bulk lifetimes from 3400 to 0.8 μs due to different initial crystal growth and thermal history. The experimental decays were all measured 200 h after oxide stripping and corresponding theoretical decays plotted with solid lines are shown. Analysis of Fig. 7 illustrates that if surface recombination dominates over the bulk, e.g., compare sample D16 ($\tau_{\text{bulk}} = 145$ μs) with sample D14 ($\tau_{\text{bulk}} = 3400$ μs), the difference in curves is very small, especially insofar as noise affects the data. Simple calculations based on Eq. (3) show that the corresponding effective lifetimes will change from 24.5 to 29.2 μs , respectively. Thus, if an effective lifetime 26.9 μs were measured with an accuracy $\Delta\tau_{\text{eff}} = \pm 8.8\%$, samples D14 and D16 would be indistinguishable due to measurement errors. Therefore, lowering of the measurement error is crucial for bulk lifetime evaluation. The full set of ex-

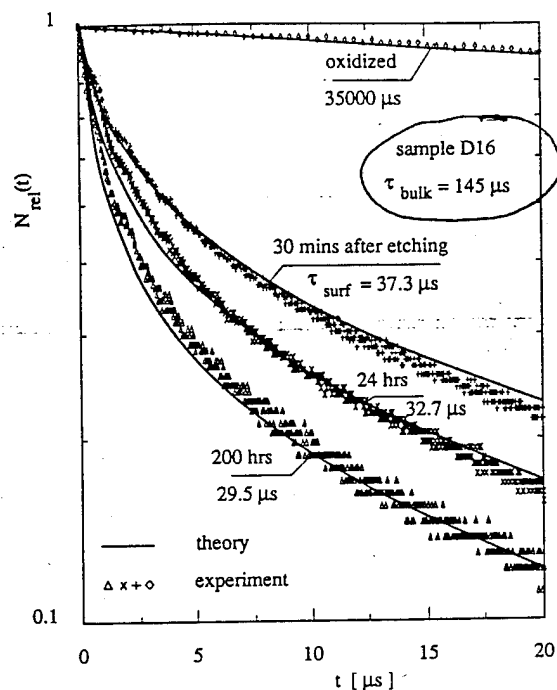


FIG. 6. Influence of different surface conditions on experimental carrier decay (points) for sample with the same bulk lifetime value, and theoretical curve fitting (solid lines).

perimental results for the wafers tested is summarized in Table I and shows that it is very difficult to recover the bulk lifetime value when surface recombination process is dominant. The averaged lifetime ranging from 0.45 to 10

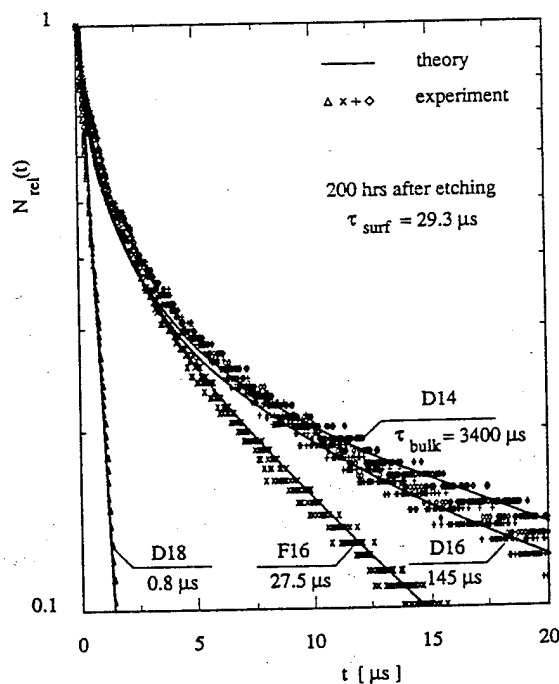


FIG. 7. Influence of bulk lifetime on experimental carrier decay (points) for samples with similar surface conditions, and theoretical curve fitting (solid lines).

TABLE I. Averaged value of lifetime components after separation procedure measured on oxidized wafers and 30 min, 24 h, and 200 h after oxide etching.

Sample	Oxidized	30 min after oxide etching				24 h after oxide etching				200 h after oxide etching			
		τ_{bulk}	τ_{eff}	S	τ_{surf}	τ_{bulk}	τ_{eff}	S	τ_{surf}	τ_{bulk}	τ_{eff}	S	τ_{surf}
		(μs)	(μs)	(cm/s)	(μs)	(μs)	(μs)	(cm/s)	(μs)	(μs)	(μs)	(cm/s)	(μs)
D14	3300.0	41.0	1480	45.1	451.0	34.1	2850	35.2	1040.0	29.2	6940	29.3	10000.0
D16	153.0	29.6	2120	38.9	124.0	26.4	3480	33.4	127.0	24.4	7200	29.1	150.0
F16	31.3	14.3	1390	46.3	21.0	13.5	3020	35.4	21.9	13.7	5750	31.6	24.6
D18 ^a	0.92	0.89	... ^a	... ^a	0.89	0.88	... ^a	... ^a	0.88	0.93	... ^a	... ^a	0.93

^aCannot be determined.

ms instead of 3.3 ms was derived, comparing values measured on oxidized sample D14 to the ones obtained after the separation procedure on etched samples. The separation algorithm works much better for medium and low values of the bulk lifetime, although the lifetime measured on oxidized wafers is always slightly longer than that recovered by the algorithm. This effect is believed to result from the requirement of low electron-hole pair generation level not being met. Thus, when oxidized wafers are measured longer lifetimes are commonly observed. For sample D18 with very short effective lifetime, the bulk of semiconductor wafer dominates the recombination process. Therefore, the surface conditions do not affect the measured lifetime, in a similar way as it was considered for sample D14 with respect to the bulk action; however now the surface lifetime cannot be satisfactorily determined.

SUMMARY

The surface and bulk components of recombination lifetime measured in a noncontact photoconductance experiment have been separated by a detailed analysis of the shape of the experimentally observed decay curve. Although the initial part of the decay is not exponential, the tail may be comfortably approximated by an exponent. The initial part depends mostly on surface recombination processes while the latter part is influenced by both surface and bulk effects. The proposed algorithm for lifetime component separation is based on measurements of the tail decay slope and its y intercept. In this work it was shown that the y intercept does not depend on the bulk lifetime but simply on the surface lifetime. However, it has to be acknowledged that for surface component calculations the diffusion constant and wafer thickness have to be known. Surface recombination velocities within the range from several hundred to several tens of thousand cm/s can be measured with the algorithm. As the advantage of this algorithm, an increased accuracy of surface lifetime recovery can be pointed out since both the y intercept and decay slope are averaged by linear fitting routine in hundreds of

experimental points. The algorithm was positively verified on a set of samples with the bulk lifetime ranging from 1 μs to 3 ms at four different surface conditions. The measurement accuracy of bulk lifetime recovery is limited by its dependence on effective and surface lifetime terms, where two reciprocals of numbers which are often very close each other, are subtracted. This limitation is common for all algorithms dealing with separation problem. Therefore, the measurement error significantly increased when the wafer was characterized by extremely long bulk lifetimes on the order of ms as expected. For the same reason, the surface component could not be satisfactorily recovered when the bulk lifetime was below a few μs value. As far as bulk lifetime is concerned, the algorithm works best on the wafers with bulk lifetime values on the order of a few hundred μs and below.

ACKNOWLEDGMENTS

We would like to acknowledge SEMITEX Co., LTD and K. Katayama for supplying the LIFETECH-88[®] system and samples, respectively. This work was partially supported by SERI Grant No. XL-8-18097.

- ¹D. K. Schroder, *Semiconductor Material and Device Characterization* (Wiley, New York, 1990), pp. 359-448.
- ²J. W. Orton and P. Blood, *Electrical Characterization of Semiconductors: Measurements of Minority Carrier Properties* (Academic, San Diego, 1990), p. 19.
- ³M. S. Tyagi, J. F. Nijs, and R. J. van Overstraeten, *Solid State Electron.* 25, 411 (1982).
- ⁴A. S. Grove, *Physics and Technology of Semiconductor Devices* (Wiley, New York, 1967), pp. 144, 334.
- ⁵K. L. Luke and L. J. Cheng, *J. Electrochem. Soc.* 135, 957 (1988).
- ⁶K. Katayama, Y. Kirino, K. Iba, and F. Shimura, *Jpn. J. Appl. Phys.* 30B, L1907 (1992).
- ⁷K. L. Luke and L. J. Cheng, *J. Appl. Phys.* 61, 2282 (1987).
- ⁸S. Eranen and M. Blomberg, *J. Appl. Phys.* 56, 2372 (1984).
- ⁹A. Buczkowski, Z. Radzinski, G. Rozgonyi, and F. Shimura, *J. Appl. Phys.* 69, 6495 (1991).
- ¹⁰K. Katayama and F. Shimura, in *Defects in Silicon II*, edited by W. M. Bullis, W. Gosele, and F. Shimura (The Electrochemical Society, Pennington, NJ, 1991), Vol. 91-9, p. 97.
- ¹¹F. Shimura, T. Okui, and T. Kusama, *J. Appl. Phys.* 67, 7168 (1990).

Effect of Ultraviolet Irradiation on Surface Recombination Velocity in Silicon Wafers

A. Buczkowski, G. A. Rozgonyi and F. Shimura

Department of Materials Science and Engineering

North Carolina State University

Raleigh, NC 27695-7916

Recombination lifetime measurements are commonly applied for electrical characterization of semiconductor materials and evaluation of crystal quality.¹ With the availability of wafers with very low defect densities and high lifetime carrier recombination processes now appear to be controlled by the surface recombination velocity (S). However, since the bulk lifetime value is desired for evaluation of material properties, the surface recombination can be an unwanted, perturbing measurement effect. Thus, in order to obtain the bulk lifetime, a separation of the surface and bulk components is obligatory; or, if possible, those practical solutions for which the surface component is negligible must be verified. For example, it is possible to reduce the surface recombination velocity either by oxidation,² or by chemical immersion during measurement.³ Recently, it has also been noticed that the surface activity can be decreased in wafers covered with a native oxide if they are illuminated with ultraviolet (UV) light.⁴ However, in this case the low surface recombination is not constant and recovers to its initial value after several tens of minutes. The physical mechanism of temporary surface deactivation is not yet fully understood; it has been postulated⁵ that during UV irradiation substrate electrons are excited over the native oxide/silicon barrier, are captured by oxygen atoms at the air/native oxide interface, and then discharge back with cooperation of ($\equiv\text{Si-OH}$) molecules. In any case, the S decrease will be related to charge captured by slow states present within the native oxide.⁶ The objective of this work is to offer theoretical support for the slow state capture explanation.

Figure 1 presents a schematic bandgap diagram of the SiO₂/Si near-surface region and introduces the physical variables to be used in subsequent calculations. Based on the analysis of A. Many et al.,⁷ and F. Berz,⁸ for a low injection approximation the surface recombination velocity as given by Eqn. 5.83 in Ref. 7 is:

$$S = \frac{\sqrt{K_n K_p} N_t (n_b + p_b)}{2 n_i \left[\cosh \left(\frac{E_t - E_i}{k T} - u_0 \right) + \cosh (v_s + u_b - u_0) \right]} \quad (1a)$$

$$u_b = \frac{E_F - E_i}{k T}, \quad v_s = \frac{V_s}{k T / q}, \quad u_0 = \ln (K_p / K_n) \quad (1b)$$

where q is the electronic charge, k - the Boltzman constant, T - the absolute temperature, n_i - the intrinsic concentration of electrons, n_b , p_b - the bulk concentration of electrons and holes, respectively, and K_n , K_p - the electron and hole capture probabilities, N_t - the surface concentration of fast states, E_F - the Fermi energy, E_t - the energy of trap, u_b - the normalized bulk potential, V_s - surface potential. Therefore, the surface recombination velocity is not solely dependent on trap properties as expressed by trap energy, concentration, and capture cross section, but is also modified by the surface potential V_s . In fact, the influence of surface potential is crucial, and a small change in V_s can vary the surface recombination by several orders of magnitude. This is illustrated in the family of curves in Fig. 2 which presents the dependence of surface recombination velocity on surface potential for p- and n-type substrates, with the trap energy as a parameter.

Returning to Ref.4 data, if UV irradiation changes the equilibrium charge state at the surface region which has a great impact on the surface recombination velocity, it will explain the experimentally observed phenomenon of lifetime variation within silicon wafers after UV exposure. In order to calculate the steady-state value of surface potential, it is assumed that the total charge Q present at the semiconductor surface consists of three components: Q_{slow} the negative charge of electrons captured within slow states during UV irradiation, Q_{fast} the negative or

positive charge of fast states at the native oxide/ silicon interface, and Q_{scr} the compensating charge of the space-charge region. Under steady-state conditions the total charge is equal to zero. Thus:

$$Q(V_s) = Q_{slow} + Q_{fast}(V_s) + Q_{scr}(V_s) = 0 \quad (2)$$

The surface potential V_s , modified by Q_{slow} , Q_{fast} and Q_{scr} charges, can be found as a root of this equation.

The Q_{fast} charge depends on concentration of fast states at the interface, their donor or acceptor nature, and occupancy status. For donor-type states the charge is positive when states are empty and neutral when occupied, while acceptors are neutral when empty and negative when filled with electrons. Therefore:

$$Q_{fast} = q N_t (1 - f_t) \quad (\text{for donor states}) \quad (3a)$$

$$Q_{fast} = -q N_t f_t \quad (\text{for acceptor states}) \quad (3b)$$

and

$$f_t = (1 + \exp \frac{E_t - E_F - q V_s}{k T})^{-1} \quad (4)$$

where f_t is the probability of state occupancy by an electron. In the following calculation it is assumed that the fast states are donor-like when located below and acceptor-like when above the midgap.² The charge Q_{slow} is arbitrarily postulated to be given by:

$$Q_{slow} \equiv -q N_{slow} \exp(-\frac{t}{t_r}) \quad (5)$$

and is based on the experimentally observed change of surface recombination velocity with time, where t_r is a relaxation constant. The charge Q_{scr} compensates the charges $Q_{fast} + Q_{slow}$, maintains the neutrality requirement as given by Eqn. 2, and is equal to:⁷

$$Q_{scr} = -\text{SGN}(V_s) \epsilon \frac{k T / q}{L_B} F_s \quad (6a)$$

where

$$L_B = \sqrt{\frac{\epsilon k T}{q^2 (n_b + p_b)}} \quad (6b)$$

is the bulk Debye length,

$$F_s = \sqrt{2 \left(\frac{\cosh(u_b + v_s)}{\cosh(u_b)} - v_s \tanh(u_b) - 1 \right)} \quad (6c)$$

the space charge function, ϵ the dielectric constant of silicon, and $\text{SGN}(V_s)$ the sign function. Finally, the effective recombination lifetime as measured, for example, with a transient photoconductance technique, can be expressed in terms of its bulk and surface components as:

$$\frac{1}{\tau_{\text{eff}}} = \frac{1}{\tau_{\text{bulk}}} + \frac{1}{\tau_{\text{surf}}} \quad (7)$$

where

$$\frac{1}{\tau_{\text{surf}}} = \alpha^2 D \quad (8)$$

with α being the first root of

$$\tan(\alpha d/2) = \frac{S}{\alpha D} \quad (9)$$

d = the wafer thickness, and D = the carrier diffusion constant.⁹

Under equilibrium conditions, i. e. $Q_{\text{slow}} = 0$, and $Q_{\text{scr}} = Q_{\text{fast}}$, the surface recombination velocity depends on N_t , the surface concentration of traps in a highly nonlinear fashion due to the previously mentioned dependence on surface potential. An example of the relationship between τ_{eff} and S versus the surface concentration of acceptor traps located at $E_t = 0$ is presented in Fig. 3 for n-type material. Note that for the p-type case presented in Fig. 3, the surface potential is practically not effected by presence of traps, while S is proportional to N_t . This occurs because the traps considered are located above the Fermi level, and remain empty and neutral. After UV irradiation, an additional charge Q_{slow} , which is time dependent, and compensated by $Q_{\text{scr}} + Q_{\text{fast}}$ must be taken into account. Therefore, we have plotted all these charge components, as derived from Eqns. 3, 5, and 6, in Fig. 4 as a function of time. Note that the surface recombination velocity is also a

function of time because of time dependence of surface potential as given by Eqns. 5 and 2. The final result of this analysis is presented in Figs. 5a and b which plots the τ_{eff} versus time for p- and n-type substrates, respectively. This dependence is in good agreement with experimental results, as presented in Ref. 6 and marked with points in Fig. 5a.

In summary, a theoretical model for the influence of UV irradiation on surface recombination velocity is proposed for experimentally observed variations of effective lifetime and surface recombination velocity with the time. The surface recombination decrease is attributed to the charging and discharging process of slow states present within the native oxide which covers the silicon wafers.

The authors would like to acknowledge L. Zhong and K. Katayama for discussion and making their experimental data available to us.

REFERENCES

- ¹ J. W. Orton and P. Blood, *Electrical Characterization of Semiconductors: Measurements of Minority Carrier Properties*, Academic Press, San Diego 1990, pg. 19.
- ² *Ionizing Radiation Effects In MOS Devices and Circuits*, eds. T. P. Ma and P. V. Dressendorfer, John Wiley & Sons, New York, pg.144, pg. 194 (1989).
- ³ K. L. Luke and L. J. Cheng, J.Electrochem. Soc., **135**, 957 (1988).
- ⁴ K. Katayama, Y. Kirino, K. Iba, and F. Shimura, Jpn. J. Appl. Phys., **30 B**, L1907 (1992)
- ⁵ K. Katayama and F. Shimura, in preparation
- ⁶ L. Zhong, A. Buczkowski, K. Katayama, and F. Shimura, in preparation
- ⁷ A. Many, Y. Goldstein, and N. B. Grover, *Semiconductor Surfaces*, North-Holland Publishing Company, Amsterdam, 128, (1965).
- ⁸ F. Berz, in *Surface Physics of Phosphors and Semiconductors*, eds. C. G. Scott and C. E. Reed, Academic Press, London, 143, (1975).
- ⁹ A. Buczkowski, Z. Radzimski, G. Rozgonyi, and F. Shimura, J. Appl. Phys., **69**, 6495 (1991)

FIGURE CAPTIONS

Fig. 1. Bandgap model of the near surface region

Fig. 2. Dependence of surface recombination velocity on surface potential for p- and n-type silicon, with trap energy as a parameter

Fig. 3. Effective lifetime, τ_{eff} and surface recombination velocity, S , versus surface concentration of acceptor traps, with trap energy $E_t = 0$, doping concentration $N_d = 10^{15} \text{ cm}^{-3}$, capture cross section $c_p = c_n = 10^{-16} \text{ cm}^2$, and bulk lifetime $\tau_{\text{bulk}} = 200 \text{ } \mu\text{s}$.

Fig. 4. Normalized charge components as a function of time, with doping concentration $N_d = 10^{15} \text{ cm}^{-3}$, trap concentration $N_t = 5 \cdot 10^{11} \text{ cm}^{-3}$, slow state concentration $N_{\text{slow}} = 1 \cdot 10^{12} \text{ cm}^{-3}$, and relaxation constant $\tau_r = 20 \text{ secs}$.

Fig. 5. Effective lifetime as a function of time, (a) p-type, and (b) n-type silicon, with relaxation time as a parameter and $N_d = 10^{15} \text{ cm}^{-3}$, trap concentration $N_t = 2.4 \cdot 10^{12} \text{ cm}^{-3}$, slow state concentration $N_{\text{slow}} = 2.2 \cdot 10^{11} \text{ cm}^{-3}$, and bulk lifetime $\tau_{\text{bulk}} = 400 \text{ } \mu\text{s}$

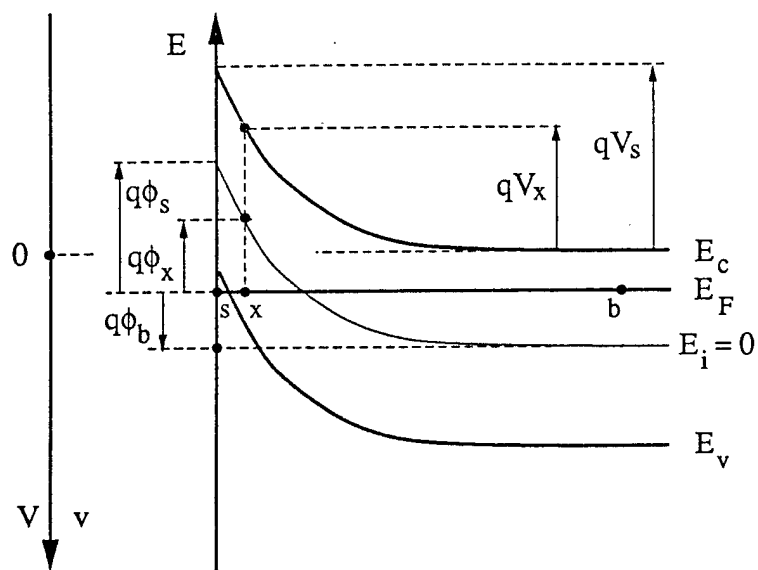


Fig. 1.

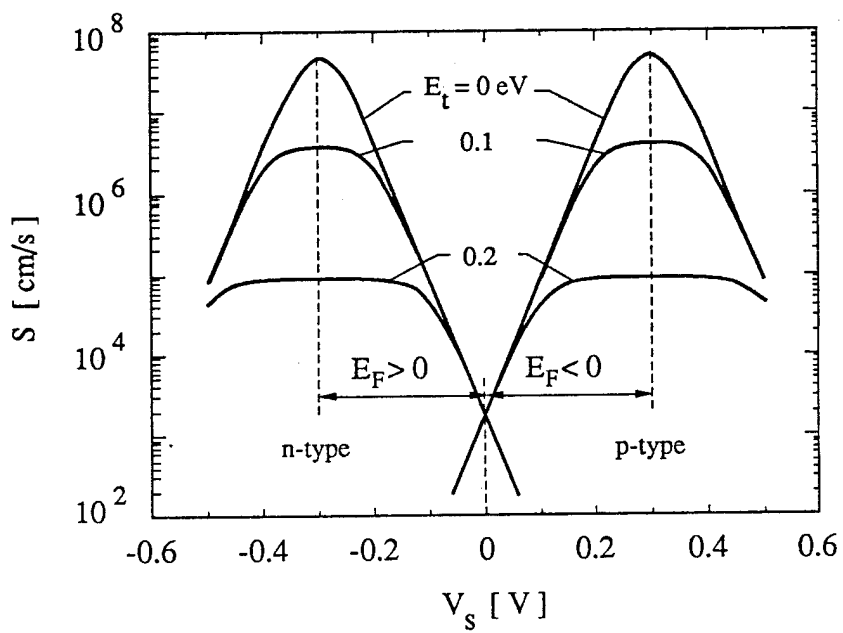


Fig. 2

Fig. 3.

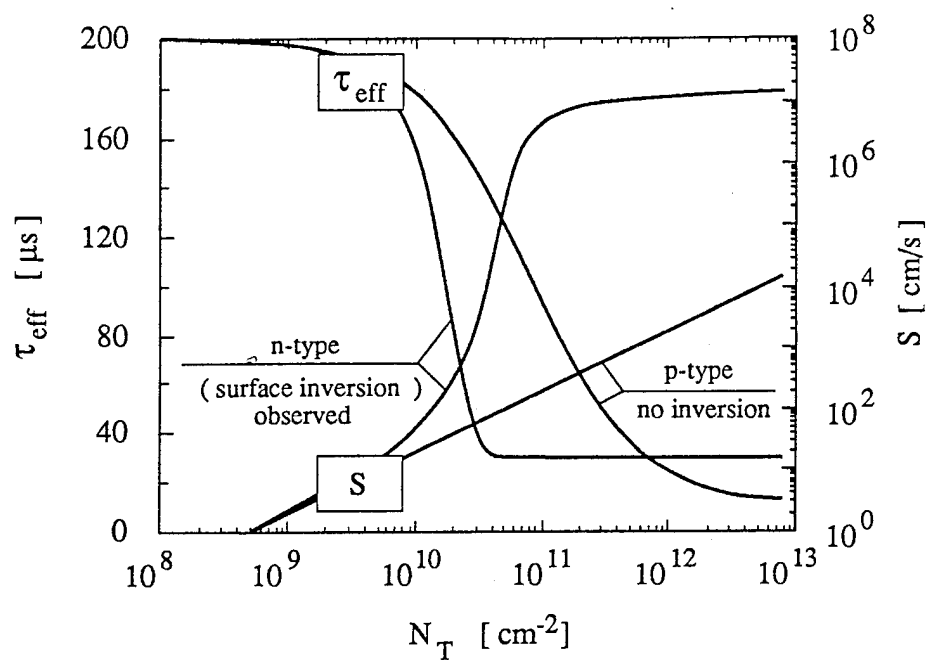


Fig. 4.

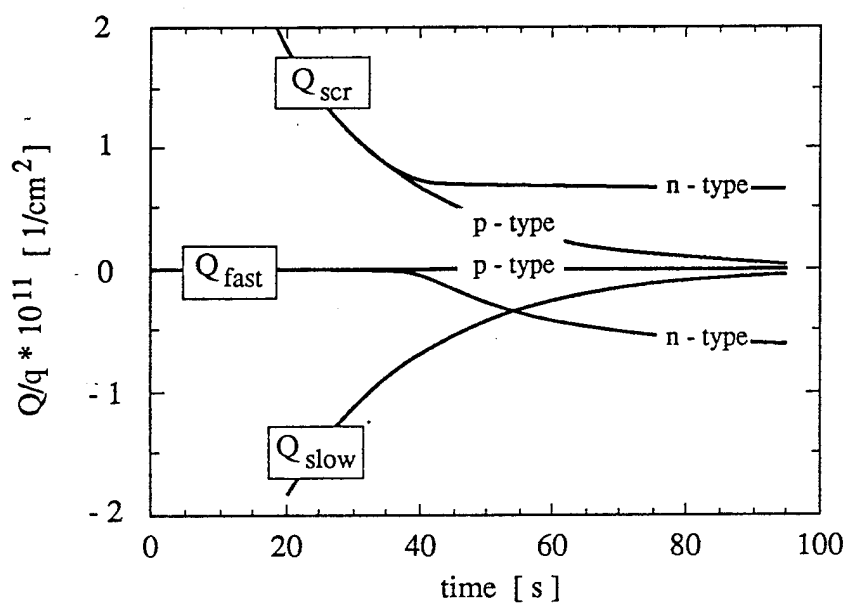


Fig. 5 a

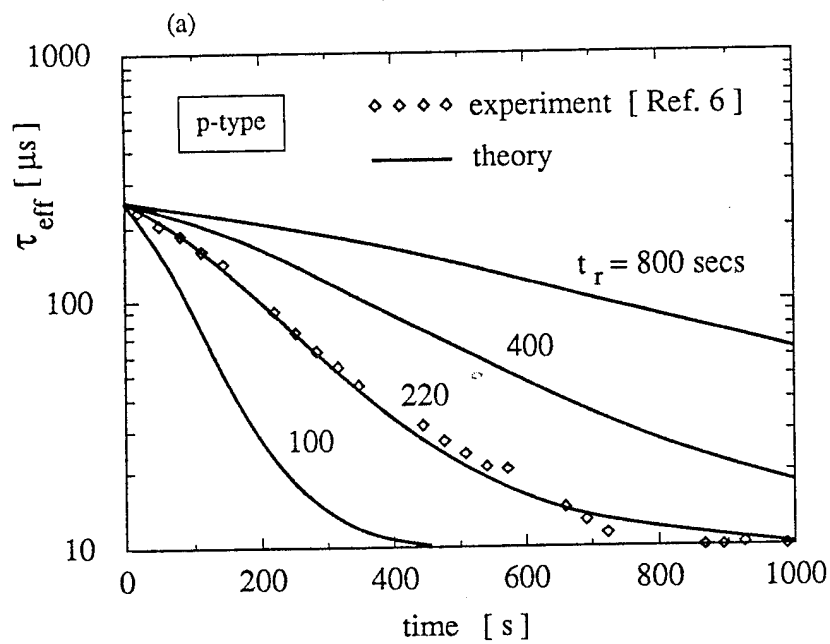


Fig. 5 b

